
5

Modeling local field potentials and their interaction with the extracellular medium

CLAUDE BÉDARD AND ALAIN DESTEXHE

5.1 Introduction

Extracellular electric potentials, such as local field potentials (LFPs) or the electroencephalogram (EEG), are routinely measured in electrophysiological experiments. LFPs are recorded using micrometer-size electrodes, and sample relatively localized populations of neurons, as these signals can be very different for electrodes separated by 1 mm (Destexhe et al., 1999a) or by a few hundred micrometers (Katzner et al., 2009). In contrast, the EEG is recorded from the surface of the scalp using millimeter-scale electrodes and samples much larger populations of neurons (Niedermeyer and Lopes da Silva, 1998). LFPs are subject to much less filtering compared to EEG, because EEG signals must propagate through various media, such as cerebrospinal fluid, dura mater, cranium, muscle and skin. LFP signals are also filtered, because the recording electrode is separated from the neuronal sources by portions of cortical tissue. Besides these differences, EEG and LFP signals display the same characteristics during wake and sleep states (Steriade, 2003).

The observation that action potentials have a limited participation in the genesis of the EEG or LFPs dates from early studies. Bremer (1938, 1949) was the first to propose that the EEG is not generated by action potentials, based on the mismatch of the time course of EEG waves with action potentials. Eccles (1951) proposed that LFP and EEG activities are generated by summated postsynaptic potentials arising from the synchronized excitation of cortical neurons. Intracellular recordings from cortical neurons later demonstrated a close correspondence between EEG/LFP activity and synaptic potentials (Klee et al., 1965; Creutzfeldt et al., 1966a, 1966b). The current view is that EEG and LFPs are generated by synchronized synaptic currents arising on cortical neurons, possibly through the formation of dipoles (Nunez, 1981; Niedermeyer and Lopes da Silva, 1998).

The fact that action potentials have little participation in EEG-related activities indicates strong frequency-filtering properties of cortical tissue. High frequencies

(greater than ≈ 100 Hz), such as that produced by action potentials, are subject to a severe attenuation, and therefore are visible only for electrodes immediately adjacent to the recorded cell. On the other hand, low-frequency events, such as synaptic potentials, attenuate less with distance. These events can therefore propagate over large distances in extracellular space and be recordable as far as on the surface of the scalp, where they can participate in the genesis of the EEG. This frequency-dependent behavior is also seen routinely in extracellular unit recordings: the amplitude of extracellularly recorded spikes is very sensitive to the position of the electrode, but slow events show much less sensitivity to the position. In other words, an extracellular electrode records slow events that originate from a large number of neighboring neurons, and are more stable to small changes of electrode position. In contrast, action potentials are recorded only for the cell(s) immediately adjacent to the electrode, and are therefore very sensitive to changes in electrode position. This property is fundamental because it allows the resolution of single units from extracellular recordings.

EEG and LFP measurements also display approximately $1/f$ frequency scaling in their power spectra (Pritchard, 1992; Novikov et al., 1997; Bhattacharya and Petsche, 2001; Bédard et al., 2006a) (see Figure 5.1). The origin of such $1/f$ “noise” is at present unclear. $1/f$ spectra can result from self-organized critical phenomena (Jensen, 1998), suggesting that neuronal activity may be working according to such states (Beggs and Plenz, 2003). Alternatively, the $1/f$ scaling may be due to filtering properties of the currents through extracellular media (Bédard et al., 2006a). This conclusion was reached by noting that the global activity reconstructed from multi-site unit recordings scales identically as the LFP if a “ $1/f$ filter” is assumed, and without the need to assume self-organized critical states in neural activity.

Despite its potential importance for resolving single cells or explaining the power spectral structure of LFPs, little is known about the physical basis of the frequency dependence of extracellular potentials in the cortex. By contrast to intracellular events, for which biophysical mechanisms have been remarkably well characterized during the last 60 years (reviewed in Koch, 1999), comparatively little has been done to investigate the biophysical mechanisms underlying the genesis of extracellular field potentials (see review by Nunez, 1981). The reason is that LFPs result from complex interactions involving many factors, such as the spatial distribution of current sources, the spatial distribution of positive and negative electric charges (forming dipoles), their time evolution (dynamics), as well as the conductive and permittivity properties of the extracellular medium. One of the simplest and widely used models of LFP activity considers current sources embedded in a homogeneous extracellular medium (Nunez, 1981; Koch and Segev, 1998). Although this formalism has been successful in many instances (Rall and

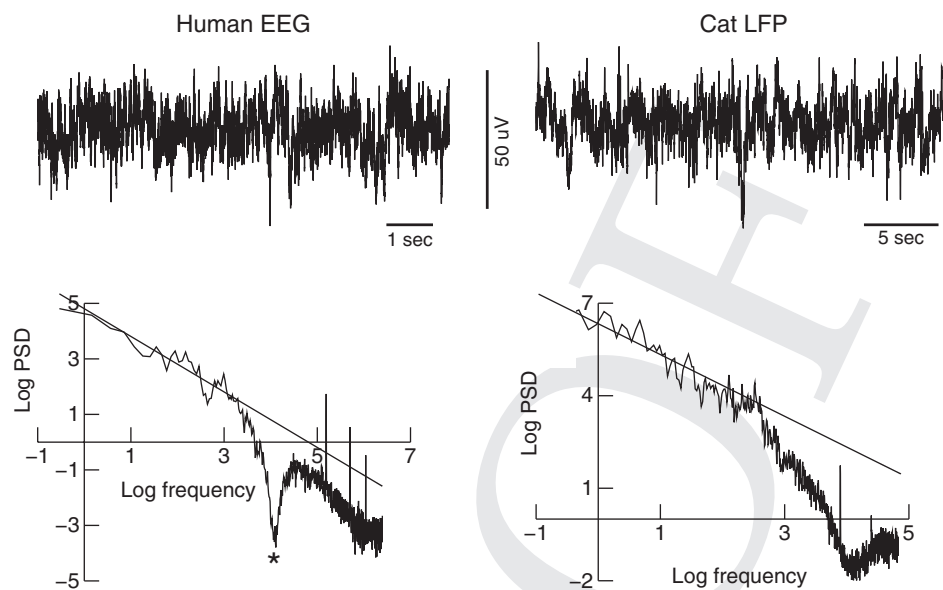


Figure 5.1 $1/f$ frequency scaling of electroencephalogram and local field potentials. The top traces show examples of human EEG recordings (left, vertex EEG) and human EEG recordings (right, parietal cortex) during awake and attentive states. The corresponding power spectral densities (lower panels) display approximate $1/f$ scaling at low frequencies. The straight lines indicate a slope of -1 in this log-log representation. The signals were not filtered, except for a notch filter at 60 Hz (*) for the EEG, and the data acquisition filters at high frequencies (not visible at this scale).

Shepherd, 1968; Klee and Rall, 1977; Destexhe, 1998; Protopapas et al., 1998), it does not account for the frequency-dependent attenuation and therefore is not precise enough to model extracellular field potentials containing both spikes and synaptic potential activity.

In this chapter, we review recent work investigating possible physical bases for the frequency-filtering properties of LFPs. We start from first principles (Maxwell equations) and consider different conditions of current sources and extracellular media. We delineate the cases leading to frequency-filtering properties consistent with physiological data. We show that the assumption of a resistive homogeneous extracellular medium cannot account for the frequency-dependent attenuation. It is necessary to take into account the inhomogeneous structure of the extracellular medium (in both permittivity and conductivity), the “reaction” of the medium (such as polarization) and ionic diffusion, in order to account for frequency-dependent attenuation.

The chapter is organized as follows: we start from the simplest model of LFPs, which consists of current sources in a homogeneous and resistive extracellular

fluid. We next consider different causes of frequency dependence, such as inhomogeneities of conductivity, polarization phenomena and ionic diffusion. We also introduce a macroscopic formalism in which all these effects can be merged together into a unified model, and finish by discussing conflicting experiments and a proposition on how to reconcile them, as well as how to reproduce the $1/f$ frequency-scaling of LFPs from plausible physical causes.

5.2 Modeling LFPs in resistive media

5.2.1 Extracellular potential in homogeneous resistive media

The simplest model for the extracellular potential assumes that the extracellular medium is purely *resistive*, with no capacitive component. In this case, one considers a set of punctual current sources embedded in a homogeneous conductive medium of conductivity σ . The extracellular potential due to a single punctual current source can be deduced simply as follows. Starting from Ohm's law ($\vec{j} = \sigma \vec{E}$), combined with the law of current conservation ($\vec{j} = \frac{i}{4\pi r^2} \hat{r}$) in spherical symmetry around the source, and by integrating along a straight line from the source to a given point in extracellular space, we obtain:

$$\begin{aligned} \Delta V(r) = V(\infty) - V(r) &= - \int_{\infty}^r \vec{E} \cdot d\vec{s} = - \frac{i}{4\pi\sigma} \int_{\infty}^r \frac{\hat{r} \cdot d\vec{s}}{r^2} \\ &= \frac{i}{4\pi\sigma} \int_{\infty}^r \frac{dr}{r^2} = - \frac{i}{4\pi\sigma} \frac{1}{r}. \end{aligned} \quad (5.1)$$

The extracellular potential at some distance r from the source i is then given by:

$$V(r) = \frac{1}{4\pi\sigma} \frac{i}{r}, \quad (5.2)$$

if we assume that the reference $V(\infty) = 0$. This relation can also be deduced directly from Coulomb's law and the first Maxwell equation in integrated form.

In the case of a set of n current sources i_j , the superposition principle applies and one can write:

$$V(r) = \frac{1}{4\pi\sigma} \sum_{j=1}^n \frac{i_j}{r_j}, \quad (5.3)$$

where r_j is the distance from the source i_j to the position r in extracellular space. This expression captures many effects such as dipoles or multipolar configurations. Equation (5.3) has been used to model extracellular potentials, from the early models (Rall and Shepherd, 1968) to today's models of extracellular activity (Protopapas et al., 1998; Nunez and Srinivasan, 2005; see also Chapter 4).

5.2.2 Example of modeling LFPs in a homogeneous resistive medium

To illustrate an example of such simple models of LFPs, we consider a model of absence seizure activity in the thalamocortical system (Destexhe, 1998). Absence seizures, like many other types of epileptic phenomena, are characterized by the genesis of typical oscillatory EEG patterns which consist of the alternation of negative sharp deflections (“spike”) and slow positive waves (“wave”), which repeats at slow frequencies (typically around 3 Hz). This “spike-and-wave” pattern is an important signature of epileptic activity (Niedermeyer and Lopes da Silva, 1998) and is seen in humans and diverse animal models, in the EEG and in the LFPs.

The thalamocortical mechanisms leading to absence seizures are complex and involve recurrent inhibition in the cortex, as well as the rebound burst properties of thalamic neurons (Destexhe et al., 1999b; Steriade, 2003). This type of activity was reproduced by biophysical models of thalamocortical networks which included the intrinsic properties of cortical and thalamic neurons, as well as the different synaptic receptors present in these circuits (Destexhe, 1998; Destexhe et al., 1999b). This model reproduced the hypersynchronized neuronal discharges in epileptic seizures, and how such activity generates the typical spike-and-wave patterns in the LFPs (Figure 5.2). In this case, the LFP was calculated using Equation (5.3), using a linear arrangement of pyramidal (PY) neurons (20 μm intercellular distance), where i_j was the transmembrane current of each pyramidal neuron, excluding the currents responsible for action potentials (see details in Destexhe, 1998). The simulation showed that spike-and-wave patterns can be reproduced by this simple model, where synchronized postsynaptic potentials (EPSP/IPSP sequences) generate the negative “spike,” while slow positive currents – also synchronized – generate the slow positive “wave” (Figure 5.2).

It is important to note that the exclusion of action potentials to generate the LFP was done here artificially. In reality, fast events (action potentials) have a much steeper attenuation compared to slow events (synaptic currents), such that only the latter contribute to the genesis of LFPs. Models with resistive media cannot account for such frequency filtering properties, and one must use more sophisticated models with non-resistive media, as we review in the next sections.

5.2.3 Multipolar configurations

Models with resistive media can also be made using multipolar source distributions. In this case, the electric potential at a point P exterior to the sources can be written as¹

¹ This expression is obtained by Taylor expansion of V around the center of charge, as a function of the inverse of the distance between point P and the center of charge.

5 Modeling LFPs and interaction with extracellular medium

141

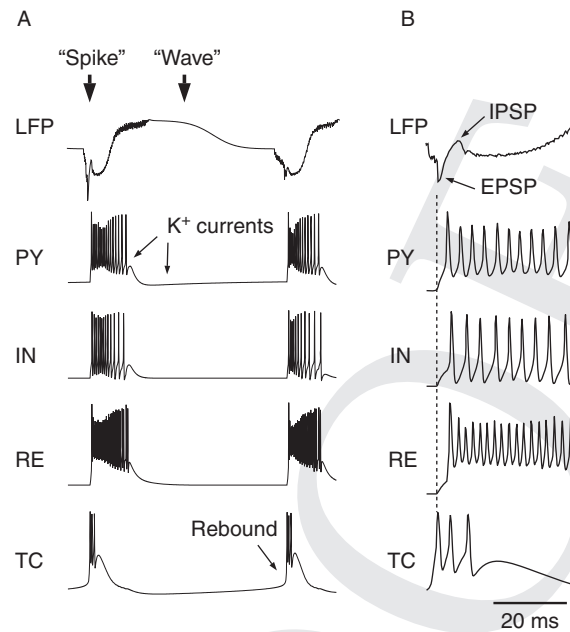


Figure 5.2 Simulation of “spike-and-wave” local field potentials in a model of absence epileptic seizures. The model consisted of a thalamocortical network where neurons were single-compartment Hodgkin–Huxley type models, and synaptic interactions were modeled by conductance-based kinetic models for glutamate (AMPA, NMDA) and γ -amino-butyric acid ($GABA_A$ and $GABA_B$) synaptic receptors. Reducing the fast ($GABA_A$ -mediated) inhibition in the cortex resulted in the emergence of hypersynchronized oscillations at a frequency of around 3 Hz. The LFP calculated from monopolar sources (pyramidal neurons only) generated the typical spike-and-wave patterns seen experimentally during seizures. When all cells fired in synchrony, the LFP generated a negative “spike,” while the neuronal silences were associated with a slow positive “wave” (A). The “spike” was generated by hypersynchronized EPSP/IPSP sequences (see magnification in B), while the “wave” was generated by slow K^+ currents in pyramidal neurons. (PY cortical pyramidal neurons, IN cortical interneurons, RE thalamic reticular neurons, TC thalamic relay cells). (Modified from Destexhe, 1998.)

$$V(\vec{r}) = \frac{1}{4\pi\epsilon} \left[\frac{Q}{r} + \frac{\hat{r} \cdot \vec{P}}{r^2} + \frac{k_0}{r^3} + \frac{k_1}{r^4} + \dots \right] \quad (5.4)$$

where $Q = \int \rho(\vec{r}') dv'$ is the total amount of charge involved in the different sources, $\vec{P} = \int \rho(\vec{r}') \vec{r}' dv'$ is the total dipole moment of the source distribution, ϵ is the electric permittivity of the medium, and r is the distance between the center of charge and point P . When the total charge (first term) is zero and the second term is non-zero, then we have a dipole by definition. We have a quadrupole when the two first terms are zero (null charge and null dipolar moment) while the third

term is non-zero. In general, we have a 2^n -pole when the n first terms are zero, while the $(n + 1)$ th term is non-zero. In the case of a dipole, for a distance r which is large compared to the spatial scale of charge distributions, the electric potential is given by:

$$V(\vec{r}) = \frac{\hat{r} \cdot \vec{P}}{4\pi\epsilon r^2}. \quad (5.5)$$

Note that $\vec{P} = q\|\vec{r}_1 - \vec{r}_2\| = qd$ when the distribution of charge is given by $q(\delta(\vec{r} - \vec{r}_1) - \delta(\vec{r} - \vec{r}_2))$. The decision to express the electrical potential as a function of charge distribution in space allows us to stress the necessity of having a variation of charge distribution in a given region of space in order to have a variation of electric field outside that region. Thus, it avoids making hypotheses on the nature of the biological sources that produce the electric field.

Although Equation (5.3) is adequate for many purposes, such as modeling extracellular spikes (see Chapter 4) or spike-and-wave patterns (Figure 5.2), this expression may be too simple for other purposes. One example is the modeling of the correct distance dependence of extracellular field potentials, or their frequency content. As we will see in the next sections, the inhomogeneities of extracellular medium have a strong impact on the propagation and frequency filtering of field potentials.

5.2.4 Is extracellular space electrically uniform?

Extracellular space is highly non-uniform, and is made from the alternation of fluids and membranes (Peters et al., 1991; see Figure 5.3). Only about 6% of the extracellular space in the cortex is devoted to interstitial space (extracellular fluid), while the core of the volume is made up of axons (34%), neuronal dendrites (35%), spines (14%) and glial cells (11%); see details in Braitenberg and Schüz (1998). Because these media have very different conductivity and permittivity, one can expect the extracellular space to be electrically highly non-homogeneous, and therefore to contradict directly Equation (5.3) which assumes homogeneity.

To integrate such inhomogeneities of extracellular space, one cannot simply use the above equations, because this would violate the assumption that σ and ϵ are constant in the Maxwell equations. Therefore, to build a model of extracellular potentials that allows variations in these parameters, one needs to start from first principles. This is the object of the next section.

5.3 Modeling LFPs in non-resistive media: general theory

In this section, we start from the Maxwell equations of electromagnetism and apply these equations to neural tissue. Because Maxwell's theory is a mean-field theory

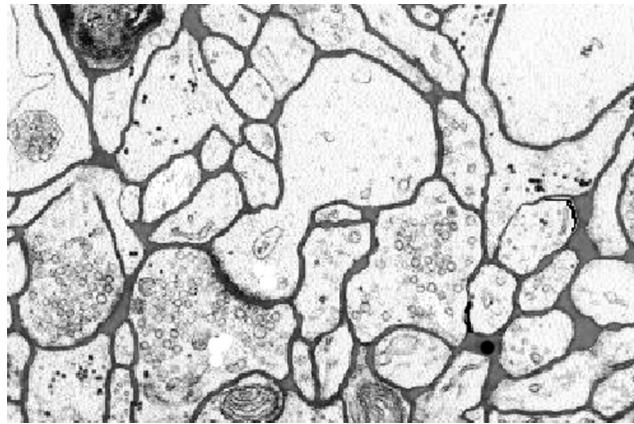


Figure 5.3 Geometry of extracellular space. Electron micrograph of a small region $4 \times 6 \mu\text{m}^2$ of rat cerebral cortex. The extracellular space (ECS) is outlined in gray. Note the simple convex cell surface and the presence of regions where the ECS widens. Note that the ECS is probably slightly reduced in width due to the fixation procedure. (Figure modified from Nicholson and Sykova, 1998.)

of electromagnetism, it is necessary to consider mean values, as we will describe below. We will model neural tissue using the three standard parameters, electric conductivity (σ), electric permittivity (ϵ) and magnetic permeability (μ).² Because neural tissue is not ferromagnetic, the magnetic permeability μ can be considered constant and equal to that of vacuum.

We derive the equations governing the time evolution of the extracellular potential for a locally neutral medium.³ We will consider two different scales: a first scale, which will be called “microscopic,” will consider averages of electromagnetic parameters (σ , ϵ , μ) over volumes of the order of cubic micrometers. These volumes are small compared to neuronal and glial processes in extracellular space. At larger scales, which will be called “macroscopic,” we will consider averages over volumes of the order of cubic millimeters, which are large compared to cellular processes.

The electromagnetic parameters have very different properties at these two scales. At microscopic scales, the conductivity is a fixed number that depends on whether a fluid or a membrane is considered. At macroscopic scales, the volumes considered contain fluids and membranes, and have capacitive effects, such as the

² It is important to note that the notions of conductivity and permittivity of a given medium do not have a physical sense at a subatomic level, and thus these notions only apply to a mean-field theory. This is analogous to the notion of pressure and temperature in classical thermodynamics.

³ We define as *locally neutral* a medium in which the charge density is zero when there is no electrical field. For the considered scales, we can assume that the neural tissue is locally neutral because these scales are large compared to the membrane thickness (around 5–7 nm), which is the value at which charge inhomogeneities will be apparent.

conductivity is a complex number in the frequency domain of Fourier analysis. However, we can treat both scales using the same formalism, as we will see below.

In the next sections, we follow a formalism similar to that developed previously (Bédard et al., 2004), except that we reformulate the model macroscopically, with frequency-dependent electrical parameters (conductivity σ and permittivity ϵ). This will allow us to integrate directly macroscopic measurements of these electric parameters, which were found to be strongly frequency dependent in some cases (Gabriel et al., 1996a, 1996b, 1996c).

5.3.1 Microscopic model

We begin by deriving a general equation for the electrical potential when the electrical parameters are scalar numbers and are frequency dependent. We start from the Maxwell equations, taking the $\nabla \cdot \vec{D} = \rho^{net}$ (Gauss' law), and $\nabla \times (\vec{B}/\mu) = \vec{j} + (\partial \vec{D}/\partial t)$ (Ampère–Maxwell law) in a medium with constant magnetic permeability, which gives:

$$\nabla \cdot \vec{D} = \rho^{net} \quad (5.6)$$

$$\nabla \cdot \vec{j} + \frac{\partial \rho^{net}}{\partial t} = 0$$

where \vec{D} , \vec{j} and ρ^{net} are respectively the electric displacement, current density and charge density in the medium surrounding the sources.

In a linear medium, the equations linking the electric field \vec{E} with electric displacement \vec{D} and with current density \vec{j} , give:

$$\vec{D}(\vec{x}, t) = \int_{-\infty}^{\infty} \epsilon(\vec{x}, \tau) \vec{E}(\vec{x}, t - \tau) d\tau \quad (5.7)$$

and

$$\vec{j}(\vec{x}, t) = \int_{-\infty}^{\infty} \sigma(\vec{x}, \tau) \vec{E}(\vec{x}, t - \tau) d\tau. \quad (5.8)$$

This model is microscopic, in the sense that the electric parameters σ and ϵ take their microscopic values and are assumed to be independent of frequency. Indeed, the electric parameters of the extracellular fluid can be considered constant for frequencies lower than 1000 Hz (Gabriel et al., 1996c). In this case, the Fourier transforms of the above equations are respectively $\vec{D}_\omega = \epsilon_\omega \vec{E}_\omega = \epsilon \vec{E}_\omega$ and $\vec{j}_\omega = \sigma_\omega \vec{E}_\omega = \sigma \vec{E}_\omega = \sigma_z \vec{E}_\omega$.⁴ It is important to note that σ_z is a real number in this microscopic model, which will not be the case in the macroscopic model of the next section.

⁴ Note that $\omega = 2\pi f$ where f is the frequency.

Given the limited precision of measurements, we can consider $\nabla \times \vec{E} \approx 0$ for frequencies smaller than 1000 Hz. Thus, we can assume that $\vec{E} = -\nabla V$ such that the complex Fourier transform of Equations (5.6) can be written as:

$$\nabla \cdot (\epsilon(\vec{x}) \nabla V_\omega) = -\rho_\omega^{net}$$

$$\nabla \cdot (\sigma(\vec{x}) \nabla V_\omega) = i\omega \rho_\omega^{net}.$$

Consequently, we have

$$\nabla \cdot ((\sigma + i\omega\epsilon) \nabla V_\omega) = \nabla(\sigma + i\omega\epsilon) \cdot \nabla V_\omega + (\sigma + i\omega\epsilon) \nabla^2 V_\omega = 0. \quad (5.9)$$

This equation was derived previously (Bédard et al., 2004) and is general enough to calculate the propagation of the extracellular potential in extracellular media which can have a complex or inhomogeneous structure, as well as frequency-dependent electric parameters.

Equation (5.9) reduces to the Laplace equation ($\nabla^2 V_\omega = 0$) when the medium is homogeneous with respect to σ and ϵ . Thus, Equation (5.9) is a generalization of the Laplace equation for a medium where σ and ϵ are non-homogeneous. Except for particular cases where the ratio ϵ/σ is independent of position, Equation (5.9) shows that, in non-homogeneous media, the extracellular potential will necessarily have a different power spectral structure compared to that of the current sources, because the extracellular potential must be solution of a differential equation with frequency-dependent coefficients.

5.3.2 Macroscopic model

In principle, it is sufficient to solve Equation (5.9) in the extracellular medium to obtain the frequency dependence of LFPs. However, in practice, this equation cannot be solved because the structure of the medium is too complex to define the limit conditions properly. The associated values of electric parameters must be specified for every point of space and for each frequency, which represents a considerable difficulty. One way to solve this problem is to consider a macroscopic or mean-field approach at a larger scale, noting that the Maxwell equations are invariant under change of scale.⁵ This approach is justified here by the fact that the values measured experimentally are averaged values, with the precision depending on the measurement technique. Because our goal is to simulate these macroscopic measurements, we will use a macroscopic model, in which we take spatial averages of Equation (5.9), and make a continuous approximation for the spatial variations of these average values (see Bédard and Destexhe, 2009).

⁵ Note that a change of scale can necessitate renormalizing electromagnetic parameters.

To this end, we define macroscopic electric parameters, ϵ^M and σ^M , as follows:

$$\epsilon_\omega^M(\vec{x}) = \langle \epsilon_\omega(\vec{x}) \rangle_V = f(\vec{x}, \omega)$$

and

$$\sigma_\omega^M(\vec{x}) = \langle \sigma_\omega(\vec{x}) \rangle_V = g(\vec{x}, \omega)$$

where V is the volume over which the spatial average is taken. We assume that V is of the order of mm^3 , and is thus much smaller than the cortical volume, so that the mean values will be dependent of the position in the cortex.

A priori, it may seem surprising here that macroscopic parameters depend on frequency. However, as we have seen in the preceding section, the independence of frequency of microscopic parameters does not imply that there is no frequency dependence macroscopically. As shown by Equation (5.9), the impedance inequalities can generate a dependence on frequency. Thus, if we replace the electric parameters of a non-homogeneous region by their mean values, we have to include parameters which depend on frequency, even if the microscopic parameters are frequency independent.

Because the average values of electric parameters are statistically independent of the mean value of the electric field, we have:

$$\begin{aligned} \langle \vec{j}^{total} \rangle_V(\vec{x}, t) &= \int_{-\infty}^{\infty} \sigma^M(\tau) \langle \vec{E} \rangle_V(\vec{x}, t - \tau) d\tau \\ &+ \int_{-\infty}^{\infty} \epsilon^M(\tau) \frac{\partial \langle \vec{E} \rangle_V}{\partial t}(\vec{x}, t - \tau) d\tau, \end{aligned}$$

where the first term on the right hand side represents the “dissipative” contribution, and the second term represents the “reactive” contribution (reaction from the medium, such as polarization). Here, all physical effects, such as diffusion, resistive and capacitive phenomena, are integrated into the frequency dependence of σ^M and ϵ^M . We will examine this frequency dependence more quantitatively in Section 5.6.

The complex Fourier transform of $\langle \vec{j}^{total} \rangle_V(\vec{x}, t)$ then becomes:

$$\langle \vec{j}_\omega^{total} \rangle_V = (\sigma_\omega^M + i\omega\epsilon_\omega^M) \langle \vec{E}_\omega \rangle_V = \sigma_z^M \langle \vec{E}_\omega \rangle_V, \quad (5.10)$$

where σ_z^M is the complex macroscopic conductivity. We can also assume

$$\sigma_z^M = i\omega\epsilon_z^M \quad (5.11)$$

such that

$$\nabla \cdot \langle \vec{j}_\omega^{total} \rangle_V = \nabla \cdot (\sigma_z^M \langle \vec{E}_\omega \rangle_V) = \nabla \cdot (i\omega\epsilon_z^M \langle \vec{E}_\omega \rangle_V) = 0. \quad (5.12)$$

5 Modeling LFPs and interaction with extracellular medium

147

Because $\sigma_z^M = (\sigma_\omega^M + i\omega\epsilon_\omega^M)$ and $\langle \vec{E}_\omega \rangle = -\nabla\langle V_\omega \rangle$, the expressions above (Equations (5.12)) can also be written in the form:

$$\nabla \cdot ((\sigma_\omega^M + i\omega\epsilon_\omega^M)\nabla\langle V_\omega \rangle|_V) = 0. \quad (5.13)$$

We note that starting from the continuum model (Bédard et al., 2004), where only spatial variations were considered, and generalizing this model by including frequency-dependent electric parameters, gives the same mathematical form as the original model (compare with Equation (5.9)). This form invariance will allow us to introduce surface polarization phenomena as well as the physical effects of ionic diffusion by including an ad hoc frequency dependence in σ_ω^M and ϵ_ω^M (see Section 5.7). The physical cause of this macroscopic frequency dependence is that the cortical medium is microscopically non-neutral (although the cortical tissue is macroscopically neutral). Such a local non-neutrality was already postulated in a previous model of surface polarization (Bédard et al., 2006a). This situation cannot be accounted for by Equation (5.9) if σ_ω^M and ϵ_ω^M are frequency independent (in which case $\rho_\omega = 0$ when $\nabla V_\omega = 0$). Thus, including the frequency dependence of these parameters enables the model to capture a much broader range of physical phenomena.

Finally, a fundamental point is that the frequency dependences of the electrical parameters σ_ω^M and ϵ_ω^M cannot take arbitrary values, but are related to each other by the Kramers–Kronig relations (Kronig, 1926; Landau and Lifshitz, 1984; Foster and Schwan, 1989):

$$\Delta\epsilon^M(\omega) = \epsilon^M(\omega) - \epsilon^M(\infty) = \frac{2}{\pi} \int_0^\infty \frac{\sigma^M(\omega')}{\omega'^2 - \omega^2} d\omega' \quad (5.14)$$

and

$$\sigma^M(\omega) = \sigma^M(0) - \frac{2\omega^2}{\pi} \int_0^\infty \frac{\Delta\epsilon^M(\omega')}{\omega'^2 - \omega^2} d\omega' \quad (5.15)$$

where principal value integrals are used. These equations are valid for any linear medium (i.e., when Equations (5.7) and (5.8) are linear). These relations will turn out to be critical for relating the model to experiments, as we will see in Section 5.8 below.

Note that, in contrast to the frequency dependence, the spatial dependences of σ_ω^M and ϵ_ω^M are independent of each other, because these dependences are related to the spatial distribution of elements within the extracellular medium.

5.3.3 Simplified geometry for macroscopic parameters

To obtain an expression for the extracellular potential in the macroscopic model, we need to solve Equation (5.13), which is possible analytically only if we consider

a simplified geometry of the source and surrounding medium. The first simplification is to consider the source as monopolar. The choice of a monopolar source does not intrinsically reduce the validity of the results because multipolar configurations can be composed from the arrangement of a finite number of monopoles (Purcell, 1984). In particular, if the physical nature of the extracellular medium determines a frequency dependence for a monopolar source, it will also do so for multipolar configurations. A second simplification is to consider that the current source is spherical and that the potential is uniform on its surface. This simplification will enable us to calculate exact expressions for the extracellular potential and should not affect the results on frequency dependence. A third simplification is to consider the extracellular medium as isotropic. This assumption is certainly valid within a macroscopic approach, and is justified by the fact that the neuropil of the cerebral cortex is made of a quasi-random arrangement of cellular processes of very diverse size (Braitenberg and Schüz, 1998). This simplified geometry will allow us to determine how the physical nature of the extracellular medium can determine a frequency dependence of the LFPs, independently of other factors (such as more realistic geometry, propagating potentials along dendrites, etc.).

Thus, considering a spherical source embedded in an isotropic medium with frequency-dependent electrical parameters, combining with Equation (5.13), we have:

$$\frac{d^2 \langle V_\omega \rangle_{|V}}{dr^2} + \frac{2}{r} \frac{d \langle V_\omega \rangle_{|V}}{dr} + \frac{1}{(\sigma_\omega + i\omega\epsilon_\omega)} \frac{d(\sigma_\omega + i\omega\epsilon_\omega)}{dr} \frac{d \langle V_\omega \rangle_{|V}}{dr} = 0. \quad (5.16)$$

Integrating this equation gives the following relation between two points r_1 and r_2 in the extracellular space,

$$r_1^2 \frac{d \langle V_\omega \rangle_{|V}}{dr}(r_1) [\sigma_\omega(r_1) + i\omega\epsilon_\omega(r_1)] = r_2^2 \frac{d \langle V_\omega \rangle_{|V}}{dr}(r_2) [\sigma_\omega(r_2) + i\omega\epsilon_\omega(r_2)]. \quad (5.17)$$

Assuming that the extracellular potential vanishes at large distances ($\langle V_\omega \rangle = 0$), we find

$$\langle V_\omega \rangle_{|V}(r_1) = \frac{I_\omega(R)}{4\pi\sigma_z(R)} \int_{r_1}^{\infty} dr' \frac{1}{r'^2} \frac{\sigma_\omega(R) + i\omega\epsilon_\omega(R)}{\sigma_\omega(r') + i\omega\epsilon_\omega(r')}, \quad (5.18)$$

where $I_\omega(R)$ is the current produced by the source and $\sigma_z(R)$ is the extracellular conductivity at the border of the spherical source. This expression is valid for both microscopic and macroscopic models for spherical symmetry. The difference between the two types of models lies in the expression for σ_z : in the microscopic model σ_z is real, while it is complex in the macroscopic model.

In the following, we will use the simplified notations \vec{j}_ω , \vec{E}_ω and V_ω instead of $\langle \vec{j}_\omega \rangle_{|V}$, $\langle \vec{E}_\omega \rangle_{|V}$ and $\langle V_\omega \rangle_{|V}$, respectively in order to keep the same formalism for both microscopic and macroscopic models.

Finally, using the relation $V_\omega = Z_\omega I_\omega$, the impedance Z_ω is given by:

$$Z_\omega(r) = \frac{1}{4\pi\sigma_z(R)} \int_r^\infty dr' \frac{1}{r'^2} \frac{\sigma_\omega(R) + i\omega \epsilon_\omega(R)}{\sigma_\omega(r') + i\omega \epsilon_\omega(r')} \quad (5.19)$$

where r is the distance between the center of the source and the position defined by \vec{r} . This expression will be used in the next sections, every time the impedance needs to be evaluated.

Note that this expression is valid only for a source and surrounding medium in spherical symmetry. This of course constitutes an approximation compared to the complex structure of biological media. This approximation enables us to treat the system analytically, and evaluate the influence of inhomogeneities of conductivity on local field potentials in a simple configuration. More complex configurations will be considered in Sections 5.5 and 5.6.

5.3.4 Different models of non-resistive media

In the rest of the chapter, we will consider different physical mechanisms giving rise to non-resistive extracellular media (still within the macroscopic model). These mechanisms involve the complex structure of extracellular media, with alternating fluids and membranes. In such media, we will successively investigate the effect of abrupt variations of impedance (fluids and membranes) in a continuum model (Bédard et al., 2004), the effect of polarization (Bédard et al., 2006a) and the effect of ionic diffusion (Bédard and Destexhe, 2009), as illustrated in Figure 5.4.

5.4 Modeling LFPs in non-resistive media: the continuum model

The simplest model of non-resistive media considers a continuum approximation of the inhomogeneities of electric parameters in extracellular space (Bédard et al., 2004). The inhomogeneous composition of extracellular space is essentially due to the alternation of fluids and membranes. This structure is represented here by *smooth* spatial profiles of variation of the electric parameters, conductivity and permittivity (σ_ω and ϵ_ω), respectively. This model is a direct application of Equation (5.19) above. To enable one to treat the problem analytically, a further assumption is that the current source is spherical, and that the spatial variations of σ_ω and ϵ_ω follow a spherical symmetry around the source or, in other words, they vary only according to the radial distance from the source. We will examine how the spatial pattern of σ and ϵ affects the frequency filtering of the LFP signal.

It is important to note that this type of model is *microscopic*, in the sense that the values of σ_ω and ϵ_ω are supposed to represent the values of conductive fluids or

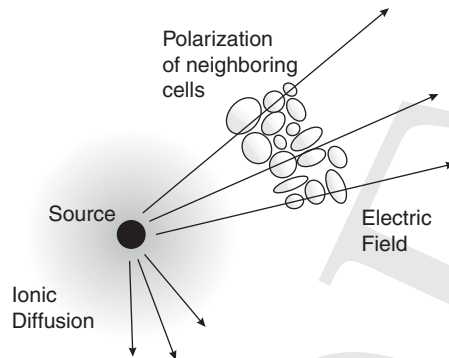


Figure 5.4 Illustration of several physical phenomena involved in the genesis of local field potentials. A given current source produces an electric field, which propagates across media consisting of fluids and membranes. The electric field will also tend to polarize the charged membranes around the source, as schematized at the top. The flow of ions across the membrane of the source will also involve ionic diffusion to re-equilibrate the concentrations. This diffusion of ions will also be responsible for inducing currents in extracellular space. These phenomena influence the frequency filtering and the genesis of LFP signals. (Modified from Bédard and Destexhe, 2009.)

membranes, at scales of the order of micrometers. The particular choices of values were those derived in Bédard et al. (2004).

We begin by considering the impedance of homogeneous media, and show that it is equivalent to a macroscopic resistance. We then discuss the order of magnitude of the electric parameters from known experimental results. Next, we present a few particular spatial profiles of $\sigma_\omega = \sigma(r)$ and $\epsilon_\omega = \epsilon(r)$ in order to illustrate how these (frequency-independent) variations can lead to frequency filtering effects. Finally, we will illustrate this frequency filtering by a numerical simulation of LFPs in a neuron model.

5.4.1 Frequency independence in homogeneous media

In an extracellular medium where the ratio ϵ/σ is constant in space, Equation (5.13) becomes (dividing by $1 + i\omega\frac{\epsilon}{\sigma}$):

$$\nabla \cdot \left[\sigma \left(1 + i\omega\frac{\epsilon}{\sigma} \right) \nabla V_\omega \right] = \nabla \cdot [\sigma \nabla V_\omega] = 0. \quad (5.20)$$

To determine the influence the frequency filtering properties of the medium, we consider a white noise source. Because the above second-order differential equation has a unique solution when the boundary conditions are specified and independent of frequency we can write that the extracellular potential is necessarily frequency independent because for boundary conditions independent of frequency

we must have the same solution for every frequency. Thus, the spatial homogeneity of ϵ/σ and the independence of σ of frequency are sufficient conditions for a frequency-independent impedance of the medium. The same applies if the ratio ϵ/σ is independent of frequency and if the medium is homogeneous.

Now we show that the above condition is also a necessary condition for frequency independence of the impedance. If we suppose that ϵ/σ depends on space, and that the extracellular potential does not depend on frequency, then Equation (5.13) is completely different for $f = 0$ and $f \neq 0$. The solution of Equation (5.13) would then depend on frequency, which is contradictory to one of the assumptions.

In the rest of the chapter, we will designate the quantity $\tau_{MW} = \epsilon_\omega/\sigma_\omega$ as the *Maxwell–Wagner time*. The physical meaning of this time, also called “dielectric time,” is the mean time taken by a given non-stationary electric charge distribution to reach equilibrium in the dielectric in the absence of an electric field (see Chapter 10 and pp. 374–375 in Maxwell, 1873; see also Raju, 2003).

We can conclude at this point that:

if one of the electric parameters is independent of frequency, then the spatial homogeneity of τ_{MW} is a necessary and sufficient condition to have a perfectly resistive medium.

Thus, in these conditions, the impedance of the extracellular medium is equivalent to a macroscopic resistance. We will show that this is not necessarily the case in neural tissue.⁶ It is interesting to note that if the medium is homogeneous with respect to τ_{MW} and σ (or equivalently with respect to σ and ϵ), then we recover the simple LFP model of Equation (5.2). In this case, Equations (5.9) and (5.19) become:

$$\nabla^2 V_\omega = 0 \quad (5.21)$$

and

$$V_\omega = Z_\omega(r)i_\omega = \frac{i_\omega}{4\pi} \int_r^\infty dr' \frac{1}{r'^2} \frac{1}{\sigma} = \frac{1}{4\pi\sigma} \frac{i_\omega}{r}. \quad (5.22)$$

In general, σ and ϵ will take very different values according to whether they represent fluids or membranes, and these values correspond to very different values of τ_{MW} (see next section). Thus, we can say that the extracellular potentials will be frequency dependent, but there is no information on whether this frequency

⁶ Note that a medium homogeneous with respect to τ_{MW} is not necessarily homogeneous relative to σ and ϵ , because these parameters could display identical spatial variations such that their ratio, τ_{MW} , remains invariant.

dependence is strong or negligible. In the next section, we evaluate this as a function of the order of magnitude of the electric parameters.

5.4.2 Conductivity and permittivity of neural tissue

Precise experimental data on the variations of permittivity ϵ_ω and conductivity σ_ω at microscopic scales in the extracellular medium have not been measured so far. However, averaged values of these parameters are available from macroscopic measurements. A value for σ_ω , averaged over large extracellular distances, σ_{av} , was measured by Ranck (1963) and was between 0.28 Sm^{-1} and 0.43 Sm^{-1} , for 5 Hz and 5 kHz, respectively. The macroscopic frequency dependence of conductivity therefore seems relatively weak. However, the situation is different microscopically. As reviewed in Nunez and Srinivasan (2005), the conductivity of the CSF fluid is 1.56 Sm^{-1} while the typical conductivity of membranes is 10^{-9} to $3.5 \times 10^{-9} \text{ Sm}^{-1}$. This value was obtained from the resting (leak) membrane conductance of cortical neurons, typically around $4.5 \times 10^{-5} \text{ S cm}^{-2}$, multiplied by the thickness of the membrane (2–8 nm; Peters et al., 1991). Other types of membranes, such as myelinated or unmyelinated fibers, and glial cells, have different membrane conductances, which are in the range of 0.1 to $10^{-6} \text{ S cm}^{-2}$ (Hille, 2001). At microscopic scales, there is therefore approximately nine orders of magnitude variation of conductivity.

The value of ϵ of a membrane is between 10^{-11} and $8 \times 10^{-11} \text{ Fm}^{-1}$. This value is derived from the specific capacitance of membranes, $C_\omega = C = 1 \mu\text{F cm}^{-2}$ (Johnston and Wu, 1999), assuming a membrane thickness of 2 to 8 nm (Peters et al., 1991). The value ϵ_ω of extracellular fluid is not known, but was roughly estimated from conductivity measurements of salted water (Gabriel et al., 1996b), which was reported to be of the order of 10^{-2} to 10^{-3} Fm^{-1} for frequencies between 10 and 100 Hz. We will see in the next section that these variations can be responsible for significant frequency filtering effects.

5.4.3 Non-homogeneous extracellular media

We have shown above that, in a homogeneous medium relative to the Maxwell–Wagner time, and if the electric parameters do not depend on frequency, the extracellular electric potential does not display frequency-dependent properties. We now turn to a possible source of frequency-dependent attenuation, namely the presence of inhomogeneities in the Maxwell–Wagner time, by varying the conductivity of the extracellular medium, while keeping a constant permittivity. We will also consider the case where both parameters vary in space.

5 Modeling LFPs and interaction with extracellular medium

153

In the following, we assume $\sigma_\omega = \sigma$ and $\epsilon_\omega = \epsilon$ and we will use normalized values for conductivity $\sigma(r)/\sigma(R)$ and permittivity $\epsilon(r)/\sigma(R)$. Because the membrane is always surrounded by extracellular fluid, the conductivity at the source is $\sigma(R) = 1.56 \text{ Sm}^{-1}$. Based on the values estimated above, in simulations we use the values for the normalized conductivity $\sigma(r)/\sigma(R)$ included between large values (equal to unity) and a low value of 2×10^{-9} . Similarly, the normalized (constant) value of permittivity will be $\epsilon(r)/\sigma(R) \approx 0.01 \text{ s}$. We have verified that no qualitative change results from variations of these parameters.

In a first example, we considered the case of a localized reduction of conductivity (Figure 5.5A) while the permittivity was kept constant $\epsilon(r)/\sigma(R) \approx 0.01 \text{ s}$. The resulting impedance measured at different distances from the source is shown in Figure 5.5A as a function of frequency f . In this case, for distances around the conductivity drop, there is a moderate frequency dependence with low-pass characteristics (Figure 5.5A, dotted and dashed lines).

Because the extracellular space is composed of alternating fluids and membranes (Peters et al., 1991), which have high and low conductivity, respectively, we next considered the situation where the conductivity fluctuates periodically with distance (Figure 5.5B). Considering a cosine function of conductivity with constant permittivity leads to a rather strong frequency-dependent attenuation with low-pass characteristics. There was a strong attenuation with distance for all frequencies (Figure 5.5B). Very similar results were obtained with other periodic functions (for example by replacing \cos by \sin in the function used in Figure 5.5B), different oscillation periods, or even for damped oscillations of conductivity (not shown).

It could be argued that although fluids and membranes alternate in extracellular space, there is efficient diffusion of ions only in the extracellular fluid around the membrane. For larger distances, diffusion becomes increasingly difficult because of the increased probability of meeting obstacles. In this case, the conductivity would be highest around the source and would decrease progressively to an “average” conductivity level for larger distances. This situation is illustrated in Figure 5.5C. We have considered, as a third example, that the conductivity is highest at the source, then decreases exponentially with distance with a space constant λ (Figure 5.5C; note that in this case, real distances were used). The resulting impedance displayed pronounced frequency filtering properties with low-pass characteristics. In particular, the attenuation with distance revealed strong differences between low and high frequencies of the spectrum (Figure 5.5C). Similar results can be obtained with other decreasing functions of connectivity (not shown).

Another example that could be considered is the case where the electric parameters σ and ϵ fall abruptly at a short distance from the source. This situation would account for the fact that the conductivity is high only in the immediate

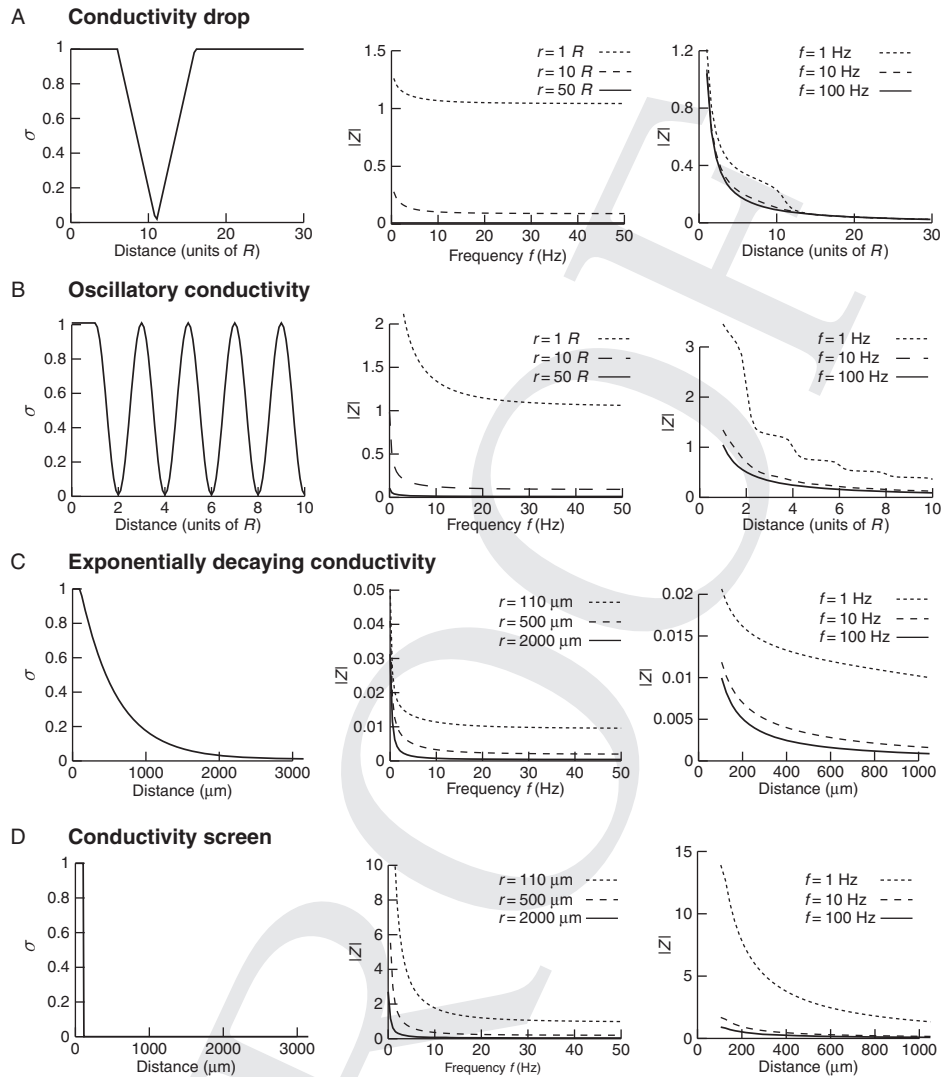


Figure 5.5 Frequency filtering properties obtained for four different profiles of spatial variation of σ . Left: spatial profile of σ shown as a function of relative distance d/R , where R is the radius of the source. Middle: impedance $|Z|$ as a function of frequency for three values of d/R (1, 10 and 100). Right: impedance as a function of distance d/R for three different frequencies (1, 10 and 100 Hz). A. Drop in conductivity. $\sigma(r)/\sigma(R) = 1 - 0.2(r - 6R)/R$ for $6R < r < 11R$, $\sigma(r)/\sigma(R) = -1 + 0.2(r - 6R)/R$ for $11R < r < 16R$, and $\sigma(r)/\sigma(R) = 1$ otherwise. B. Oscillatory conductivity. $\sigma(r)/\sigma(R) = 0.501 + 0.5 * \cos[2\pi(r - R)/2R]$. C. Exponentially decaying conductivity. $\sigma(r)/\sigma(R) = \sigma_0 + (1 - \sigma_0) \exp[-(r - R)/\lambda]$, with a space constant $\lambda = 500 \mu\text{m}$ and $\sigma_0 = 10^{-9} \text{Sm}^{-1}$. D. Abrupt variation of conductivity. $\sigma(r)/\sigma(R) = 1$ and $\epsilon(r)/\sigma(R) = 0.01$ for $r < 100 \mu\text{m}$, while $\sigma(r) = 10^{-9}$ and $\epsilon(r)/\sigma(R) = 10^{-11} \text{ s}$ for $r > 100 \mu\text{m}$. Permittivity is constant in A–C, with $\epsilon(r)/\sigma(R) = 0.01 \text{ s}$.

neighborhood of the source, in the extracellular fluid, and drops abruptly at a distance corresponding to the position of the membrane of neighboring cells. This configuration also gave frequency dependence (not shown).

5.4.4 Comparison of different conductivity profiles

The above examples show that there can be a strong frequency filtering behavior, with low-pass characteristics as observed in experiments. However, although these examples show a more effective filtering for high frequencies, it still remains to be shown that the high frequencies attenuate more steeply with distance compared to low frequencies. To this end, we define the quantity:

$$Q_{100} = Z_{100}(r)/Z_1(r), \quad (5.23)$$

where Z_1 and Z_{100} are the impedances computed at 1 Hz and 100 Hz, respectively. This ratio quantifies the differential filtering of fast and slow frequencies as a function of distance r . Figure 5.6A displays the Q_{100} values obtained for some of the examples considered above. In the case of a localized drop in conductivity (Figure 5.5A, *Drop*), there was an effect of distance for $r < 16R$, then the Q_{100} remained equal to unity for further distances. This behavior is in agreement with the impedance shown in Figure 5.5A, in which case there was no frequency filtering for $r > 16R$. For oscillatory conductivities (Figure 5.6, *Osc*), Q_{100} was always less than unity, consistent with the low-pass frequency filtering behavior observed

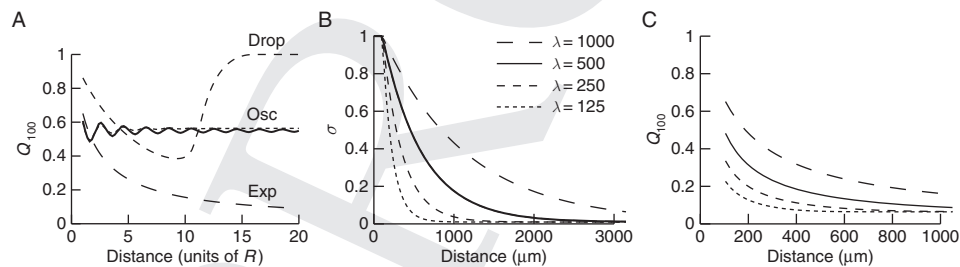


Figure 5.6 Distance dependence of frequency filtering properties. A. Ratio of impedance at fast and slow frequencies (Q_{100}) represented as a function of distance r (units of R). The Q_{100} ratios are represented for different profiles of conductivity. *Drop*: localized drop in conductivity (short dash; same parameters as in Figure 5.5A). *Osc*: oscillatory profile of conductivity (solid line; same parameters as in Figure 5.5B); the dotted line indicates a damped cosine oscillation). *Exp*: exponential decrease in conductivity (long dash; same parameters as in Figure 5.5C except $R = 1$, $\lambda = 10R$). B. Profiles of conductivity with exponential decay (same parameters as in Figure 5.5C; space constants λ indicated in μm). C. Q_{100} ratios obtained for the conductivity profiles shown in B.

in Figure 5.5B. However, Q_{100} oscillated around a value of 0.6 and did not decrease further with distance. Thus, in this case, although there was a clear low-pass filtering behavior, all frequencies still contribute by the same relative amount to the extracellular potential, regardless of distance. On the other hand, with exponential decay of conductivity, Q_{100} decreased monotonically with distance (Figure 5.6, *Exp*). Thus, this case shows both low-pass filtering behavior (Figure 5.5) and a stronger attenuation of high frequencies compared to low frequencies (Figure 5.5C, *Exp*), which is in qualitative agreement with experiments. Analyzing exponentially decaying conductivities of different space constants (Figure 5.6B) revealed that the various patterns of distance dependence approximately followed the pattern of conductivity (Figure 5.6C). This type of conductivity profile is relatively simple and plausible, and will be the one considered in the biophysical model investigated in Section 5.4.5.

If the conductivity and permittivity fall abruptly at a short distance λ from the source (Figure 5.5D), the Q_{100} value is independent of distance for $r > \lambda$, while at large distances it is approximately equal to the Q_{100} value of the exponentially decaying conductivity (not shown).

5.4.5 Biophysical model of the frequency-filtering properties of local field potentials

We now apply the above formalism to model the frequency dependence of the extracellular field potentials stemming from a conductance-based spiking neuron model (Figure 5.7). We consider a simple biophysical model of a spiking neuron containing voltage-dependent and synaptic conductances. The single-compartment model neuron includes conductance-based models of voltage-dependent conductances and synaptic conductances. This model is described by the following membrane equation:

$$C_m \frac{dV}{dt} = -g_L(V - E_L) - g_{Na}(V - E_{Na}) - g_{Kd}(V - E_K) - g_M(V - E_K) - g_e(V - E_e), \quad (5.24)$$

where $C_m = 1 \mu\text{F cm}^{-2}$ is the specific membrane capacitance, $g_L = 4.52 \times 10^{-5} \text{ S cm}^{-2}$ and $E_L = -70 \text{ mV}$ are the leak conductance and reversal potential. $g_{Na} = 0.05 \text{ S cm}^{-2}$ and $g_{Kd} = 0.01 \text{ S cm}^{-2}$ are the voltage-dependent Na^+ and K^+ conductances responsible for action potentials and were described by a modified version of the Hodgkin and Huxley (1952) model. $g_M = 5 \times 10^{-4} \text{ S cm}^{-2}$ is a slow voltage-dependent K^+ conductance responsible for spike-frequency adaptation. $g_e = 0.4 \mu\text{S}$ is a fast glutamatergic (excitatory) synaptic conductance. The

5 Modeling LFPs and interaction with extracellular medium

157

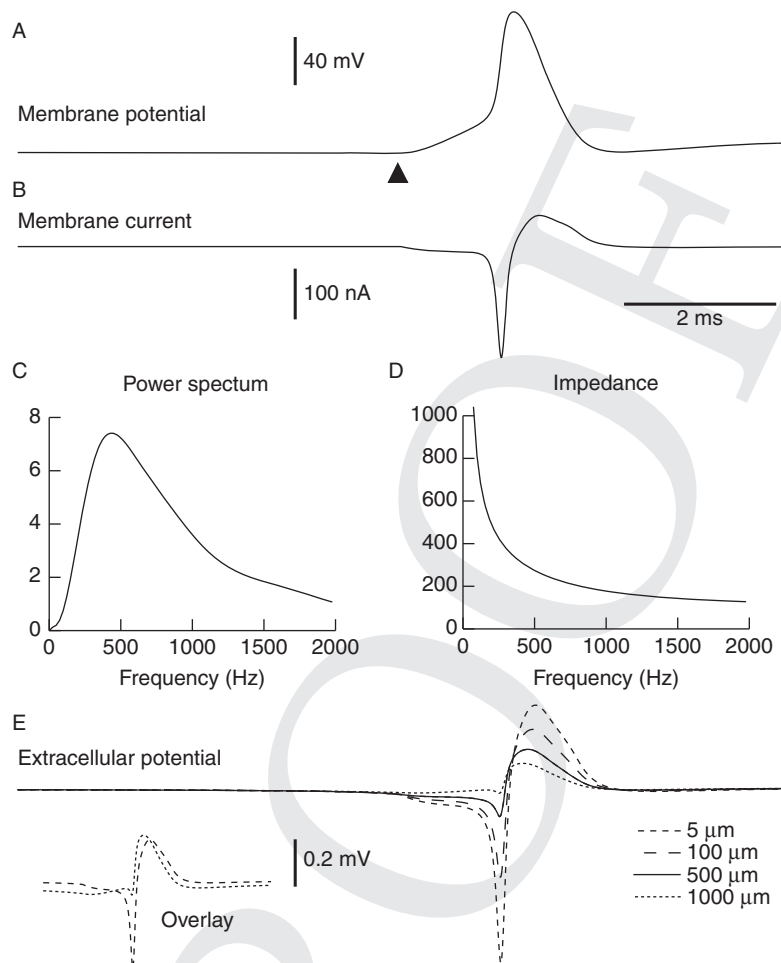


Figure 5.7 Frequency-filtered extracellular field potentials in a conductance-based model. A. Membrane potential of a single-compartment model containing voltage-dependent Na^+ and K^+ conductances and a glutamatergic synaptic conductance. The glutamatergic synapse was stimulated at $t = 5$ ms (arrow) and evoked an action potential. B. Total membrane current generated by this model. Negative currents correspond to Na^+ and glutamatergic conductances (inward currents), while positive currents correspond to K^+ conductances (outward currents). C. Power spectrum of the total current shown in B. D. Impedance at 500 μm from the current source assuming a radial profile of conductivity and permittivity. E. Extracellular potential calculated at various distances from the source (5, 100, 500 and 1000 μm). The frequency filtering properties can be seen by comparing the negative and positive deflections of the extracellular potential. The fast negative deflection almost disappeared at 1000 μm whereas the slow positive deflection was still present. The inset in E (*Overlay*) shows the traces at 5 and 1000 μm overlaid (only the amplitude was scaled).

voltage-dependent conductances are described by conventional Hodgkin–Huxley type models adapted for modeling neocortical neurons, and the synaptic conductance is described by a first-order kinetic model of neurotransmitter binding to postsynaptic receptors. These models and their kinetic parameters were described in detail in a previous publication (Destexhe and Paré, 1999), and all numerical simulations were performed using the NEURON simulation environment (Hines and Carnevale, 1997).

The profile of conductivity and permittivity used in the model is shown in Figure 5.5C. We calculate the total membrane current generated by a single-compartment model of an adapting cortical neuron, containing voltage-dependent Na^+ and K^+ conductances for generating action potentials and a slow voltage-dependent K^+ conductance responsible for spike-frequency adaptation. The model contained a fast glutamatergic excitatory synaptic conductance, which was adjusted to evoke a postsynaptic potential just above threshold, in order to evoke a single action potential (Figure 5.7A). The total membrane current (Figure 5.7B) was calculated and stored in order to calculate its Fourier transform (power spectral density shown in Figure 5.7C). The impedance of the extracellular medium (Figure 5.7D) was calculated using absolute values of the parameters (Equation (5.19)).

We now use this model to calculate the field potentials at different radial distances assuming the neuron is a spherical source (radius of 105 μm). The extracellular potential is indicated for 5, 100, 500 and 1000 μm away from the source (see Figure 5.7E) and strong frequency filtering properties are apparent: the fast negative deflection of extracellular voltage shows a steep attenuation and almost disappeared at 1000 μm (although it has the highest amplitude at 5 μm). In contrast, the slow positive deflection of the extracellular potential shows less attenuation with distance and becomes dominant at large distances (500 and 1000 μm in the example of Figure 5.7E). This is best seen from the overlaid traces (see Figure 5.7E, inset), showing the marked difference in fast and slow components in the field potentials recorded at 5 and 1000 μm .

Thus, this example illustrates that the approach provided here can lead to a relatively simple model for calculating local field potentials with frequency filtering properties. The exact profiles of filtering and attenuation depend on the exact shape of the gradients of conductivity/permittivity as well as on the spherical symmetry inherent to this model. This is illustrated in Figure 5.8 for the other radial profiles of conductivity considered earlier (drop, periodic and damped conductivity). This figure shows that for these particular profiles, the attenuation of fast and slow deflections is similar (the global shape of the LFP remains similar although attenuated in amplitude; see the almost perfect overlay in the inset of Figure 5.8C). There is therefore a negligible frequency-dependent attenuation in these cases. This is in agreement with the quasi-absence of frequency-dependent attenuation evidenced in

5 Modeling LFPs and interaction with extracellular medium

159

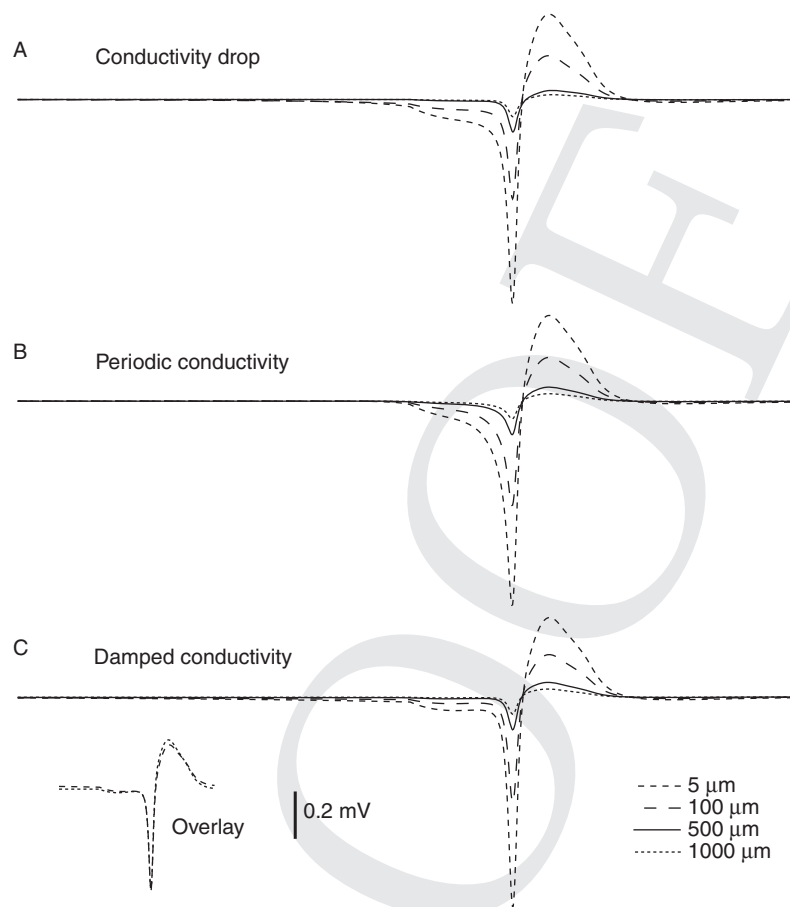


Figure 5.8 Frequency-filtered extracellular field potentials for different radial profiles of conductivity. The extracellular potential was calculated from a conductance-based spiking neuron model (identical to that of Figure 5.7) and was shown at various distances from the source (5, 100, 500 and 1000 μm) for different profile of conductivity. A. Localized drop in conductivity (constant conductivity, dropping between $r = 120 \mu\text{m}$ and $r = 280 \mu\text{m}$, as described in Bedard et al., 2004). B. Same simulation using a periodic conductivity profile (periodic function with same extremal values as in Figure 5.7 and a period of 2 μm). C. Same simulation using damped oscillations of conductivity (same parameters as in B, with a space constant of $\lambda = 500 \mu\text{m}$). In all cases, the attenuation of the fast negative deflection was similar to the slow positive deflection, in contrast with Figure 5.7E. The inset in C (*Overlay*) shows the traces at 5 and 1000 μm overlaid, which are almost superimposable (compare with inset in Figure 5.7E).

the quantitative analysis of Figure 5.6 (see above). In contrast, Figure 5.7E shows that a radial model with exponentially decaying conductivity replicates the experimental observation that only slow frequencies propagate through large extracellular distances.

5.5 Modeling LFPs in non-resistive media: the polarization model

A second type of approach to modeling the non-resistive properties of extracellular media is to include another physical phenomenon, electric polarization (Bédard et al., 2006a). In this approach, we also consider that the extracellular medium is non-homogeneous, but we assume an explicit structure consisting of a current source, surrounded by a number of other cellular processes,⁷ all surrounded by a conductive fluid. The effect of the electric field will be to polarize these cells, as illustrated in Figure 5.4.

It is important to note that in this section we consider the movement of charges in volumes of the order of cubic nanometers. This scale corresponds to the surface polarization phenomena on membranes of cells in the neighborhood of the sources. At this scale, the medium cannot be considered as locally neutral (typical membrane thickness is around 7 to 8 nm), because local excesses of charge will appear. This would not be the case for example at larger scales of μm^3 . At nanometer scales, the general equations (Equations (5.13) and (5.19)), which were introduced for a locally neutral medium, cannot apply directly. However, we will see in Section 5.7 that it is still possible to use these general equations to simulate the polarization effects of neighboring cells and its consequences on the frequency dependence of current propagation in extracellular media. The “trick” will be to consider the system as locally neutral, but incorporate an appropriate frequency dependence in the electric parameters (Bédard and Destexhe, 2009).

Indeed, a consequence of the polarization mechanisms is that the medium is considered as “reactive” in the sense that it will react to the electric field. Neighboring cells maintain charge distributions around their membrane, and these charges will be affected by the electric field and they will polarize. In other words, a given current source will necessarily polarize the medium around it, and in particular will shift the charges on the membrane surface of its neighbors. Thus, when the smallest considered scale is of the order of μm^3 , the medium can be considered as approximatively neutral, except for some small spatial fluctuations.

Not only will the medium react by polarizing, but this polarization is not instantaneous and will take a characteristic time to operate. This time, known as the *Maxwell–Wagner time*, represents the inertia of charge movement (Pethig, 1979; Raju, 2003). Thus, the frequency dependence of the electric parameters σ and ϵ , as caused by the inertial time τ_{MW} (Maxwell–Wagner time) of polarization phenomena does not vanish, even at a scale (approximately μm^3) where the medium can appear as locally neutral ($\rho \approx 0$) at all times.

⁷ We will consider these neighboring cellular processes as “passive” cells, in the sense that they maintain a membrane potential. Such processes include axons, dendrites, somas, spines, glial cells and astrocytes, all of which are part of the neuropil.

Thus, the values of the apparent (macroscopic) electric parameters at μm^3 scales necessarily have a frequency dependence which comes from this inertia time. This frequency dependence is a function of the magnitude of frequencies with respect to $1/\tau_{MW}$. We will examine the phenomenon of polarization of cell surfaces, which is not at all taken into account by models with resistive media. We will show that it does affect the propagation of field potentials.

In a first step, we will illustrate this with a simple model of surface polarization taken from a previous study (Bédard et al., 2006a). This simple model will be used to determine the frequency dependence of polarization. In a second step, we will present an application of this model in the case of a spherical current source, surrounded by different layers of adjacent cells. In a third step, we will show that the non-instantaneous character of surface polarization is important and is responsible for a form of frequency dependence. It also affects the propagation of field potentials over large distances.

5.5.1 A simple model of cell surface polarization

Neurons are characterized by various voltage-dependent and synaptic ion channels, and they will be considered here as the sole source of the electric field in extracellular space. On the other hand, glial cells are very densely packed in interneuronal space, sometimes surrounding the soma or the dendrites of neurons (Cajal, 1909; Peters et al., 1991). Glial cells normally do not have dominant voltage-dependent channel activity, rather they play a role in maintaining extracellular ionic concentrations. Like neurons, they have an excess of negative charges inside the cell, which is responsible for a negative resting potential (for most central neurons, this resting membrane potential is around -60 to -80 mV). They will be considered here as “passive” and representative of all non-neuronal cell types characterized by a resting membrane potential. We will show that such passive cells can be polarized by the electric field produced by neurons. This polarization has an inertia and a characteristic relaxation time which may have important consequences for the properties of propagation of local field potentials. These different cell types are separated by extracellular fluid, which plays the role of a conducting medium, i.e. allows for the flow of electric currents. In the remainder of this text, we will use the term “passive cell” to represent the various cell types around neurons, but bearing in mind that they may represent other neurons as well.

Another simplification is that we will consider these passive cells to be of elementary shape (spherical or cubic). Under such a simplification, it will be possible to treat the propagation of field potentials analytically and design simulations using standard numerical tools. Our primary objective here is to explore one essential physical principle underlying the frequency filtering properties of

extracellular space, based on the polarization of passive membranes surrounding neuronal sources. We assume that such a principle will be valid regardless of the morphological complexity and spatial arrangement of neurons and other cell types in extracellular space. As a consequence of these simplifications, the present work does not attempt to provide a quantitative description but rather an exploration of first principles that could be applied in later work to the actual complexity of biological tissue.

The arrangement of charges in our model is schematized in Figure 5.9A, where we delimited five regions. The membrane of the passive cell (region 3) separates the

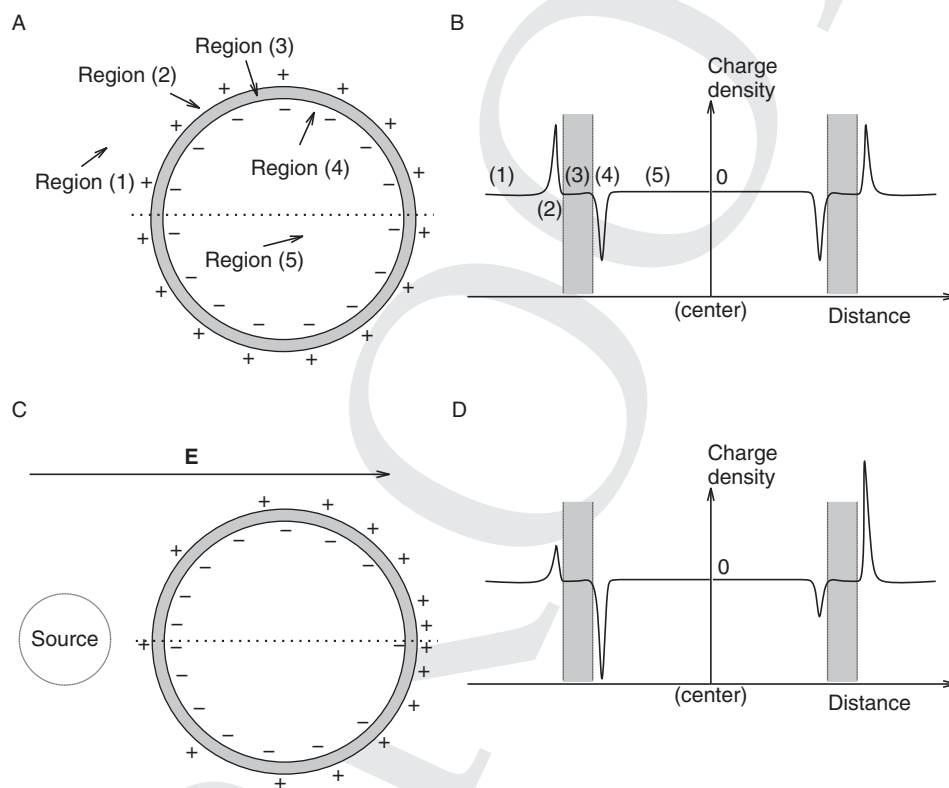


Figure 5.9 Scheme of charge distribution around the membrane of a passive cell. A. Charge distribution at rest. The following regions are defined: the extracellular fluid (region 1), the region immediately adjacent to the exterior of the membrane where positive charges are concentrated (region 2), the membrane (region 3, in gray), the region immediately adjacent to the interior of the membrane where negative charges are concentrated (region 4), and the intracellular (cytoplasmic) fluid (region 5). B. Schematic representation of the charge density as a function of distance (along the horizontal dotted line in A). C. Redistribution of charges in the presence of an electric field. The ions move away from or towards the source, according to their charge, resulting in polarization of the cell. D. Schematic representation of the charge density predicted from C.

intracellular fluid (region 5) from the extracellular fluid (region 1), both of which are electrically neutral. The negative charges in excess in the intracellular medium agglutinate in the region immediately adjacent to the membrane (region 4), while the analogous region at the exterior surface of the membrane (region 2) contains the positive ions in excess in the extracellular space. This arrangement results in a charge distribution (schematized in Figure 5.9B) which creates a strong electric field inside the membrane and a membrane potential.

The behavior of such a system depends on the values of conductivity and permittivity in these different regions (they are considered constant within each region). The extracellular fluid (region 1) has good electric conductance properties. We have taken as conductivity $\sigma_1 = 4 \Omega^{-1} \text{ m}^{-1}$, consistent with biological data $\sigma = 3.3 - 5 \Omega^{-1} \text{ m}^{-1}$, taken from measurements of specific impedance of rabbit cerebral cortex (Ranck, 1963). This value is comparable to the conductivity of salt water ($\sigma_{sw} = 2.5 \Omega^{-1} \text{ m}^{-1}$). The permittivity is given by $\epsilon_1 = 70 \epsilon_0$, corresponding to salt water. Here $\epsilon_0 = 8.854 \times 10^{-12} \text{ F m}^{-1}$ denotes the permittivity of the vacuum. In region 2, to our best knowledge, there are no experimental data on conductivity close to the membrane. We have chosen the values of $\sigma_2 = 0.7 \times 10^{-7} \Omega^{-1} \text{ m}^{-1}$ and $\epsilon_2 = 1.1 \times 10^{-10} \text{ F m}^{-1} \approx 12\epsilon_0$ for region 2. Such a choice is not inconsistent with biological observations. First, electron microscopic photographs taken from the region near the membrane reflect very little light, which hints at quite low conductivity compared to the conductivity of region 1. We consider it plausible that the permittivity in region 2 should be smaller than that in region 1. Our choice of σ_2 and ϵ_2 corresponds to a Maxwell time τ_M yielding a cut-off frequency $f_c \approx 100 \text{ Hz}$, which was also the choice given in a previous study investigating signal propagation along cable structures (bedard and Destexhe, 2008).⁸

For passive cells, we neglect ion channels and pumps located in the membrane, which is equivalent to assuming the absence of any electric current across the membrane. Therefore, region 3 has zero conductivity perpendicular to the membrane surface. The capacity of a cellular membrane has been measured and is about $C = 10^{-2} \text{ F m}^{-2}$ (Johnston and Wu, 1999). Approximating the membrane by a parallel plate capacitor (with surface area S and distance d , obeying $C = \epsilon S/d$), one estimates the electric permittivity of the membrane to be $\epsilon_3 = 10^{-10} \text{ F m}^{-1}$. Hence we used the parameters $\sigma_3 = 0$, and $\epsilon_3 = 12\epsilon_0$.

Thus, the basic idea behind the model is as follows. As represented in Figure 5.9, we consider a single spherical passive cell under the influence of an electric field. The electric field will induce a polarization of the cell by reorganizing its charge distribution (Figure 5.9C, D). This polarization will create a secondary electric field, with field lines connecting these opposite charges. It is customary to call the

⁸ Note that the value of the cut-off frequency could possibly vary according to cell type. To estimate such a cut-off, one would need to estimate the tangential resistivity, which has never been done experimentally.

original electric field the *source field*, or the *primary field*, while the field due to polarization is called the *induced field*, or the *secondary field*. The physical electric field is the sum (in the sense of vectors) of both the source and the induced fields. This induced field will be highly dependent on frequency, for high frequencies, the “inertia” of charge movement in regions 2 and 4 will limit such a polarization, and will reduce the effect of the induced field. This phenomenon is the basis of the model of frequency-dependent local field potentials presented in this section.

5.5.2 Frequency dependence of the polarization model

We now examine the frequency dependence of the secondary field produced by surface polarization. We still consider the simple case of one layer of passive cells surrounding the source. It can be shown that a very good approximation of the transfer function⁹ is given by the following expression (see Bédard et al., 2006a):

$$F_{TM}(\vec{x}, \omega) = \frac{1}{1 + i\omega\tau_{MW}} \quad (5.25)$$

where $\tau_{MW} = \epsilon^S/\sigma^S$ is the characteristic time for the inertia of surface polarization. It is important to note that ϵ^S and σ^S are the *tangential* conductivity and permittivity, respectively, and that they are therefore related to the membrane and not the extracellular medium. The physical interpretation of τ_m^S is the characteristic time to set charges into movement during the polarization; this charge movement is not instantaneous ($\tau_{MW} = 0$ would mean an infinite conductivity or zero permittivity). It is important to note that we consider here that all membranes have a unique τ_{MW} , but in reality this value may vary as a function of the molecular composition of the membrane.

The simulations (Figure 5.10) show that the induced potential vanishes for very high frequencies of the source field, a fact that can also be deduced from Equation (5.25). In other words, for very high frequencies ($\gg \tau_{MW}^{-1}$), the extracellular field will be equal to the source field, since the induced field will vanish. The space dependence is easy to deduce in such a case, and the extracellular potential attenuates with distance according to a $1/r$ law (for a spherical source), as if the source was surrounded only by conducting fluid.

However, for very low frequencies ($\ll \tau_{MW}^{-1}$), the space dependence of the extracellular potential will be a complex function depending on both the $1/r$ attenuation

⁹ The transfer function is given by:

$$F_{TM}(\vec{x}, \omega) = \lim_{t \rightarrow \infty} \frac{V_{ind}^{\omega}(\vec{x}, t) \exp(-i\omega t)}{V_{ind}^{\omega=0}(\vec{x}, t)}.$$

This function gives the ratio of the amplitude of the secondary field at a given frequency, with the amplitude of the null frequency in Fourier analysis.

5 Modeling LFPs and interaction with extracellular medium

165

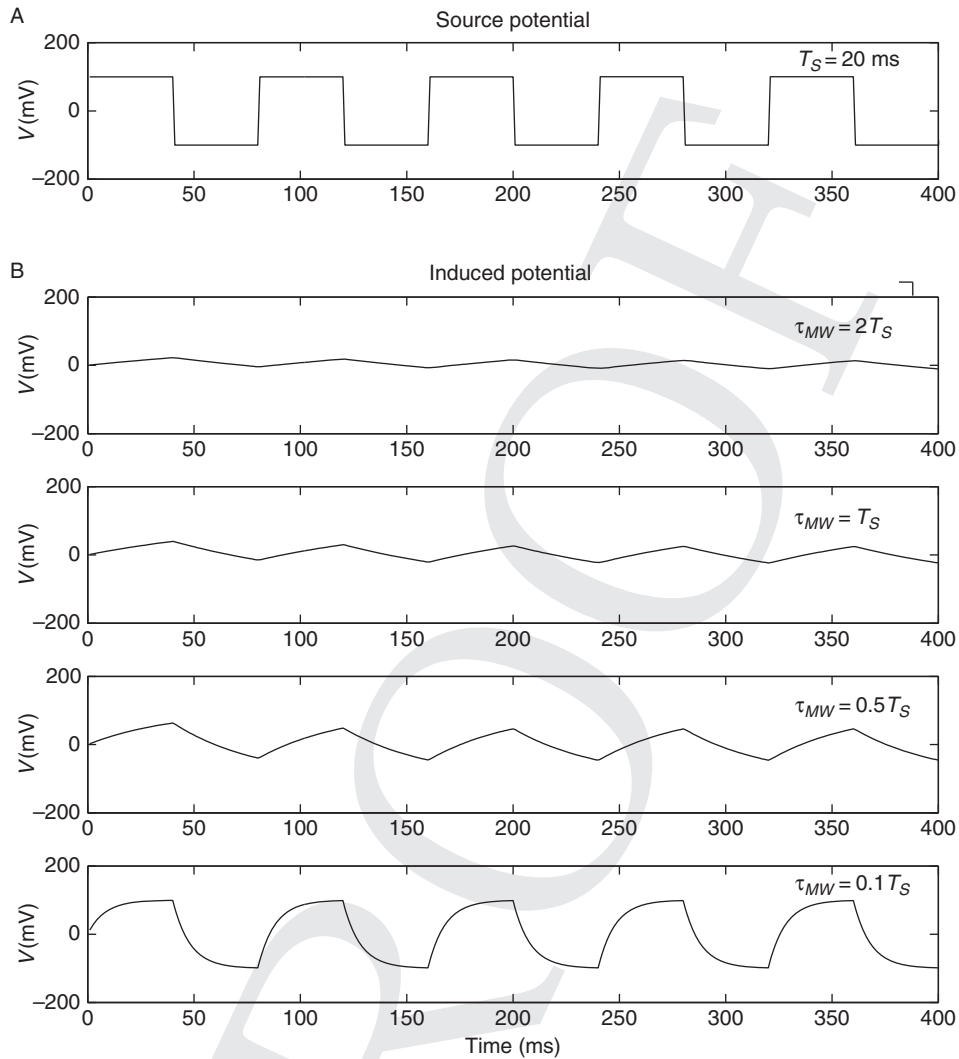


Figure 5.10 Time dependence of induced electric potential in response to an external source given by a periodic function. A. Source potential given by a periodic step function $H(\sin(\omega t))$, with period $T_S = 2\pi/\omega = 20$ ms. B. Induced electric potential for various values of T_S/τ_{MW} . In the case $T_S/\tau_{MW} \ll 1$ (top), the induced potential fluctuates closely around the mean value of the source potential. In the case $T_S/\tau_{MW} \gg 1$ (bottom) the induced potential relaxes and fluctuates between $V_{min} = 0$ mV and $V_{max} = 100$ mV of the source potential. As a result, the amplitude of oscillation becomes more attenuated with increased τ_{MW} with respect to T_S .

of the source field, and the contribution from the induced field. Such a space dependence is not easy to deduce, since it depends on the spatial arrangement of fluids and membranes around the source.

5.5.3 Attenuation as a function of distance

In this section, to illustrate the importance of surface polarization on the propagation of local field potentials, we derive the low-frequency space dependence alluded to above for a simplified arrangement of source and surrounding cells. We consider a system of densely packed and regularly arranged cells, as illustrated in Figure 5.11A.

To constrain the behavior to low frequencies, we only consider the zero-frequency limit by using a constant source field. We proceeded in two steps. First, we calculate the electric potential at the surface of a passive cell (Section 5.5.3.1). Second, we calculate the spatial profile of LFPs in a system of densely packed spheres of identical shape (Section 5.5.3.2).

5.5.3.1 Electric potential at the surface of passive membranes at equilibrium

Let us assume a spherical passive cell embedded in a perfect dielectric medium, and exposed to a constant electric field. At equilibrium, we have seen above that the effect of the electric field is to polarize the charge distribution at the surface of the cell, such as to create a secondary electric field (see Figure 5.9B), but the induced electric field is zero inside the cell. In this case, the conservation of charges on the surface implies:

$$\int_{Surf} \rho_{Surf} dS = 0, \quad (5.26)$$

where ρ_{Surf} is the charge density on the surface of the cell. The resulting electric potential is given by:

$$V_{tot}(x, y, z) = V_{source}(x, y, z) + \int_{Surf} \frac{\rho_{Surf}}{4\pi\epsilon r} dS \quad (5.27)$$

where V_{source} is the electric potential due to the source field, V_{tot} is the total resulting electric potential due to the source field and the induced field, and r is the distance from point (x, y, z) to the center of the cell. Because at the center of the cell, (a, b, c) , we necessarily have $r = R$ (where R is the cell's radius), the value of the resulting electric potential at the center is given by:

$$V_{tot}(a, b, c) = V_{source}(a, b, c) + \int_{Surf} \frac{\rho_{Surf}}{4\pi\epsilon R} dS = V_{source}(a, b, c). \quad (5.28)$$

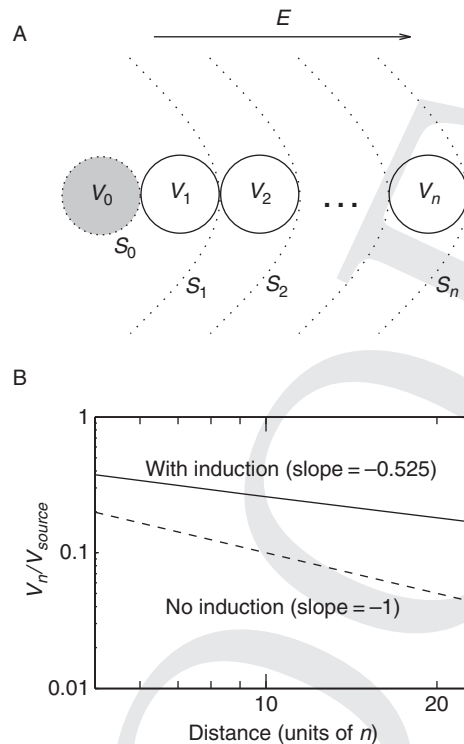


Figure 5.11 Extracellular potentials as a function of distance for a system of densely packed spherical cells. A. Scheme of the arrangement of successive layers of identical passive cells packed around a source (in gray). The potential of the source is indicated by V_0 . V_1, V_2, \dots, V_n indicate the potential at the surface of passive cells in layers 1, 2, ..., n , respectively. The dotted lines indicate isopotential surfaces, which are concentric spheres centered around the source, and which are indicated here by S_1, S_2, \dots, S_n . B. Extracellular potential as a function of distance (in units of cell radius), comparing two cases: with induction (solid line, corresponding to the arrangement schematized in A), and without induction (dashed line, source surrounded by conductive fluid only). The two cases predict a different scaling of the electric potential with distance (see text for details).

Thus, the electric potential at the surface of a spherical passive cell at equilibrium equals the potential due to the primary field at the center of the cell. In other words, the effect of the secondary field in this case perfectly compensates for the distance dependence of the primary field, such that the surface of the cell becomes isopotential, as discussed above.

5.5.3.2 Attenuation of electric potential in a system of packed spheres

Keeping the assumption of a constant electric field, we now calculate how the extracellular potential varies as a function of distance in a simplified geometry.

We consider a system of packed spheres as indicated in Figure 5.11A. From the solution of Laplace's equation, the extracellular potential at a distance r from the source center is given by:

$$V(r) = \frac{k}{r}, \quad (5.29)$$

where k is a constant, which is evaluated from the potential at the surface of the source (S_0 in Figure 5.11A),

$$V(R) = V_0 = \frac{k}{R}, \quad (5.30)$$

where R is the radius of the source. Thus, the potential due to the source field at a given point r in extracellular space is given by:

$$V(r) = \frac{R V_0}{r}. \quad (5.31)$$

Considering the arrangement of Figure 5.11A, if all cells of a given layer are equidistant from the source, their surface will be at the same potential (see Section 5.5.3.1), which we approximate as a series of isopotential concentric surfaces (S_1, S_2, \dots, S_n in Figure 5.11A). A given layer (n) of isopotential cells is therefore approximated by a new spherical source of radius r_n , which will polarize cells in the following layer ($n + 1$). According to such a scheme, the potential in layer $n + 1$ is given by:

$$V_{n+1} = \frac{r_n V_n}{d_{n+1}}, \quad (5.32)$$

where d_{n+1} is the distance from the center of cells in layer ($n + 1$) to the center of the source. According to the scheme of Figure 5.11A, we have $r_n = (2n + 1)R$ and $d_n = 2nR$. Thus, we can write the following recurrence relation:

$$V_{n+1} = \frac{2n + 1}{2n + 2} V_n. \quad (5.33)$$

Consequently:

$$V_{n+1} = \left(\prod_{j=1}^n \frac{2j + 1}{2j + 2} \right) V_0, \quad (5.34)$$

which can be written, for large n

$$V_n = \frac{(2n + 1)!}{2^{2n}(n + 1)!n!} V_0 \approx \frac{2(2n)!}{2^{2n}(n!)^2} V_0. \quad (5.35)$$

Using Stirling's approximation, $n! \simeq (n/e)^n \sqrt{2\pi n}$ for large n , leads to:

$$V_n \simeq \frac{2}{\sqrt{\pi n}} V_0. \quad (5.36)$$

Thus, in a system of densely packed spherical cells, the extracellular potential falls off like $1/\sqrt{r}$ (Figure 5.11B, continuous line).

In contrast, in the absence of passive cells in extracellular space, the electric potential is given by the source field only (Equation (5.31)), which, using the same distance notation as above, is given by:

$$V_{n+1} = \frac{V_0}{2(n+1)}. \quad (5.37)$$

Such $1/r$ behavior is illustrated in Figure 5.11B (dashed line). Note that other theories predict a steeper decay. For instance the Debye–Hückel theory of ionic solutions (Debye and Hückel, 1923) predicts a fall off as $\exp(-kr)/r$.

Thus, for this particular configuration, there is an important difference in the attenuation of extracellular potential with distance. The extracellular potential in a system of densely packed spheres falls off approximately like $1/\sqrt{r}$, in contrast to a $1/r$ behavior in a homogeneous extracellular fluid. Note that a $1/\sqrt{r}$ behavior can also be found in a system in which the source is defined as a current. For a constant current source I_0 , with variations of conductivity following a spherical symmetry around the source, the extracellular potential is given by (Bédard et al., 2004):

$$V(r) = \frac{I_0}{4\pi} \int_r^\infty \frac{1}{r^2 \sigma(r)} dr, \quad (5.38)$$

where $\sigma(r)$ is the radial profile of conductivity around the source. Assuming that $\sigma(r) = \sigma_0/\sqrt{r}$, gives

$$V(r) = \frac{\sigma_0 I_0}{4\pi \sqrt{r}} = \sqrt{\frac{R}{r}} V_0. \quad (5.39)$$

Consequently, the $1/\sqrt{r}$ behavior found above is functionally equivalent to a medium with conductivity varying like $1/\sqrt{r}$. This “effective conductivity” is similar to that introduced in Section 5.3.

5.5.4 Polarization of isotropic disorganized media

In the preceding section, we considered a very “organized” medium consisting of regularly arranged cells of the same size. Such an arrangement is of course very different from the “disorganized” arrangement of cells and fluids seen in actual neural tissue (Peters et al., 1991). In this section, we show that the phenomenon of surface polarization implies that the first layer of cells around a given source forms

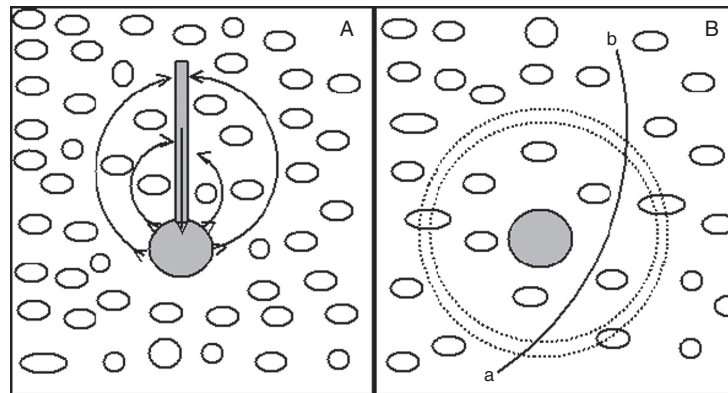


Figure 5.12 Monopole and dipole arrangements of current sources. A. Scheme of the extracellular medium containing a quasi-dipole (gray) representing a pyramidal neuron, with soma and apical dendrite arranged vertically. B. Illustration of one of the monopoles of the dipole. The extracellular space is represented by cellular processes of various size (circles) embedded in a conductive fluid. The dashed lines represent equipotential surfaces. The line \hat{ab} illustrates the fact that the extracellular fluid is linearly connex.

a perfect screen to the electric field produced by the source, but this is only the case for a “disorganized” medium. This conclusion is very different from that of the preceding section.

Let us now determine for zero frequency the amplitude of the secondary field \vec{E}_0^s produced between two cells embedded in a given electric field. First, we assume that it is always possible to trace a continuous path which links two arbitrary points in the extracellular fluid (see Figure 5.12B). Consequently, the domain defined by extracellular fluid is said to be *linearly connex*. In this case, the electric potential arising from a current source is necessarily continuous in the extracellular fluid. Second, in a first approximation, we can consider that the cellular processes surrounding sources are arranged randomly (as opposed to being regularly structured) and their distribution is therefore approximately isotropic. Consequently, the field produced by a given source in such a medium will also be approximately isotropic. Also consequent to this quasi-random arrangement, the equipotential surfaces around a spherical source will necessarily cut the cellular processes around the source (Figure 5.12B).

Because in complex Fourier analysis, the partials of the spectrum correspond to asymptotic states ($t \rightarrow \infty$), the zero-frequency component implies that the value of the charge is independent of time inside the cell (for a passive membrane). Thus, for zero frequency, there is a constant charge on cell surfaces such that the surface polarization is at steady state. This implies that the electric field inside the cells is zero (otherwise one would have a charge migration towards cell surface, which

is in contradiction with the constant charge). Therefore, there cannot be a voltage difference between two equipotential surfaces (illustrated in Figure 5.12B). One can therefore conclude that *a passive inhomogeneous medium with randomly distributed passive cells is a perfect dielectric at zero frequency*. In this case, the conductivity must tend to zero when the frequency tends to zero. Thus, in the applications considered in Section 5.7, we assume that $\vec{E}_0^S = -\vec{E}_0^P$ where \vec{E}_0^P is the field produced by the source.

5.6 Modeling LFPs in non-resistive media: the diffusion model

In this section, we consider another possible source for frequency dependence of extracellular potentials: ionic diffusion. The opening of ion channels will create ion fluxes, which will induce ionic diffusion to re-establish the local concentrations. This movement of charged particles will create an ionic diffusion current. We will show below that this contribution is significant for local field potentials, and in particular for their frequency dependence. Ionic diffusion can account for $1/f$ filtering effects for spherical current sources.

5.6.1 Is ionic diffusion important for local field potentials?

To estimate whether ionic diffusion has a potential influence on LFPs, we estimate the ratio between ionic diffusion currents (perpendicular to the membrane) and the electric field currents in the extracellular space directly adjacent to the source. We will designate this ratio by the term r_{ie} .

We have in general

$$\vec{j}_{Total} = eD\nabla[C] + \sigma\nabla V, \quad (5.40)$$

where the first term on the right hand side is the electric current density produced by ionic diffusion, while the second term is that produced by differential Ohm's law.

For a displacement $\Delta r = 10\text{nm}$ in the direction across the membrane (from inside to outside), we have approximately:

$$\vec{j}_{Total} \cdot d\vec{r} \simeq \vec{j}_{Total} \cdot \vec{\Delta r} = eD\Delta[C]_{\Delta r=10\text{nm}} + \sigma\Delta V_{\Delta r=10\text{nm}}. \quad (5.41)$$

Suppose that we have a spherical cell of $10\ \mu\text{m}$ radius, at resting potential and embedded in sea water. The resting membrane potential is a dynamic equilibrium between inflow and outflow of charges, in which these two fluxes are equal on (temporal) average. Fluctuations of current around this average in the extracellular medium around the membrane have all the characteristics of thermal noise (Nyquist, 1928) because the shot noise (see Vasilyev, 1983; Buckingham, 1985) is

zero when the current is zero on average, such that the net charge on the external side of the membrane varies around a mean value with the same characteristics as white noise (thermal noise). These fluctuations will therefore also be present at the level of the membrane potential. In this section, we evaluate the order of magnitude of the electric current caused by ionic diffusion, relative to the electric field for this situation of dynamic equilibrium.

First, the ratio between the membrane voltage noise and the variation of total charge concentration is given by

$$\Delta Q_{tot} = C \Delta V_{membrane} = k_1 \Delta V_{membrane} = 1.25 \times 10^{-11} \Delta V_{membrane}, \quad (5.42)$$

because the cell's capacitance is given by $C = 4\pi R^2 C_m = 0.04\pi R^2$ where $C_m = 10^{-2} \text{ F m}^{-2}$ is the specific capacitance of cellular membranes.

Second, mass conservation imposes

$$\Delta Q_{tot} = e \cdot v_{eff} \cdot \Delta[C]_{tot}, \quad (5.43)$$

where $e = 1.69 \times 10^{-19} \text{ C}$ and v_{eff} is the volume of the spherical shell containing the charges. Because the charges are not distributed uniformly inside the cell, but rather distributed within a thin spherical shell adjacent to the membrane, because the electric field developed across the membrane is very intense (of the order of $\frac{70 \times 10^{-3}}{7 \times 10^{-9}} \text{ V m}^{-1} = 10^7 \text{ V m}^{-1}$), Thus, the width of the shell is of the order of $dR \simeq 10^{-4} R < 1 \text{ nm}$, where the volume of the spherical shell is approximately equal to $4\pi R^2 dR$. In this case, we have for monovalent ions ($|z| = 1$)

$$\Delta Q_{tot} = k_2 \Delta[C]_{tot} \simeq 2.2 \times 10^{-38} \Delta[C]_{tot} = 2.2 \times 10^{-38} \Delta[C]_{\Delta r=10nm} \quad (5.44)$$

if we assume that the variation of concentration on the adjacent border of the exterior surface of the cell is over a width of 10 nm.

In this case, we have

$$\frac{\Delta[C]_{\Delta r=10nm}}{\Delta V_{membrane}} = \frac{k_1}{k_2} \simeq 10^{27} \text{ C m}^{-3} \text{ V}^{-1}. \quad (5.45)$$

Third, the potential difference between the cell surface and 10 nm away from it, is given by

$$\Delta V_{\Delta r=10nm} = \Delta V_{membrane} - \frac{R \Delta V_{membrane}}{R + \Delta r} \simeq 10^{-3} \Delta V_{membrane}. \quad (5.46)$$

Consequently, and assuming that the electric conductivity of the extracellular fluid is close to that of sea water (2 S m^{-1}), the ratio between the ionic diffusion current and electric diffusion current caused by thermal noise is given by:

$$r_{ie} \approx \frac{e D_{sea} \Delta[C]_{\Delta r=10nm} \Delta t}{\sigma_{\omega}^{sea} \Delta V_{\Delta r=10nm}} = \frac{e D_{sea} k_1}{\sigma_{\omega}^{sea} k_2} \simeq \frac{10^2}{\sigma_{\omega}^{sea}}, \quad (5.47)$$

where the diffusion constant of K^+ or Na^+ in sea water is of the order of $10^{-9} \text{ m}^2\text{s}^{-1}$. This implies that the ratio r_{ie} is much larger than 1 for frequencies less than 1000 Hz because σ_{ω}^{sea} of sea water is necessarily less than 2 S m^{-1} .

Because tortuosity is given by $\lambda = \sqrt{D_{sea}/D_{cortex}}$, and is between 1.6 and 2.2 (for small and large molecules, respectively) in the cerebral cortex (Nicholson and Sykova, 1998; Rusakov and Kullmann, 1998; Nicholson, 2005), the macroscopic diffusion constant in the cortex is certainly larger than $D_{sea}/10$. Thus, we have

$$r_{ie}^{cortex} > \frac{10}{\sigma_{\omega}^{cortex}} \quad (5.48)$$

where $\sigma_{f=100 \text{ Hz}}^{cortex} \simeq 0.1 \text{ Sm}^{-1}$ (see Gabriel et al., 1996c).

This evaluation shows that the phenomenon of ionic diffusion has a determinant effect and must be taken into account to calculate the current field in the cortex.

Finally, we note that we did not need to evaluate the absolute magnitude of ΔV . This evaluation is valid for a physical situation where we have a permanent white noise over a distance of 10 nm, independently of the intensity of this noise (which in practice will depend on many factors, such as the size of the cell, the number of ion channels, etc.).

5.6.2 Frequency scaling of ionic diffusion

We now calculate the frequency dependence of an ionic diffusion current outside a spherical current source. We consider a constant variation of ionic concentration, ΔC_i , on the surface of the source, and null variation at an infinite distance (Warburg conditions).

The diffusion equation for a given ionic species is

$$\frac{\partial \Delta C_i}{\partial t} = D_i \nabla^2 \Delta C_i, \quad (5.49)$$

where ΔC_i is the perturbation of the concentration C_i of ion i around the steady-state value, and D_i is the associated diffusion coefficient. This diffusion coefficient depends on the ionic species considered and the structure of the medium.

Because the geometry of the problem and the boundary conditions respect spherical symmetry, we use spherical coordinates. In this coordinate system, we have

$$\frac{\partial \Delta C_i}{\partial t} = D_i \left[\frac{\partial^2 \Delta C_i}{\partial r^2} + \frac{2}{r} \frac{\partial \Delta C_i}{\partial r} \right] \quad (5.50)$$

because ΔC_i does not depend on θ and Φ (spherical symmetry).

The Fourier transform of ΔC_i with respect to time gives:

$$\frac{\partial^2 C_{i\omega}}{\partial r^2} + \frac{2}{r} \frac{\partial \Delta C_{i\omega}}{\partial r} = \frac{d^2 C_{i\omega}}{dr^2} + \frac{2}{r} \frac{d \Delta C_{i\omega}}{dr} = \frac{i\omega}{D_i} \Delta C_{i\omega} \quad (5.51)$$

with general solution given by

$$\Delta C_{i\omega} = A(\omega) \frac{e^{\sqrt{\frac{i\omega}{D_i}} r}}{r} + B(\omega) \frac{e^{-\sqrt{\frac{i\omega}{D_i}} r}}{r}. \quad (5.52)$$

For a variation of concentration at the source border which is independent of frequency and which satisfies the Warburg hypothesis (the variation of concentration tends to zero at an infinite distance (Taylor and Gileadi, 1995; Diard et al., 1999), we have:

$$\Delta C_{i\omega}(r) = \Delta C_{i\omega}(R) \cdot \frac{R e^{-\sqrt{\frac{i\omega}{D_i}} (r-R)}}{r} \quad (5.53)$$

where r is the distance to the center of the source and R is the radius of the source.

Thus, the electric current density produced by ionic diffusion is given by:

$$\vec{j}_{i\omega}(r) = ZeD_i \frac{\partial \Delta C_{i\omega}}{\partial r} \hat{r} = -ZeD_i \left(\frac{1}{r} + \sqrt{\frac{i\omega}{D_i}} \right) \Delta C_{i\omega}(r) \hat{r} \quad (5.54)$$

where Ze is the charge of ions i , and \hat{r} is a unit vector in the direction of the current. This current is in the direction of \hat{r} by spherical symmetry.

Because we can consider that the source and extracellular medium form a spherical capacitor, the voltage difference between the surface of the source and infinite distance is given by $ZeC_p \Delta C_{i\omega}(R)$ where C_p is the capacitance value. Thus, the electric impedance of the medium is given by:

$$Z_\omega = \frac{C_p}{D_i(1/R + \sqrt{i\omega/D_i})}. \quad (5.55)$$

For a source of radius $R = 10 \mu\text{m}$ and a macroscopic ionic diffusion coefficient of the order of $10^{-11} \text{ m}^2 \text{ s}^{-1}$, and for frequencies greater than 1 Hz, we can approximate the impedance by:

$$Z_\omega \approx \frac{C_p}{\sqrt{i\omega D_i}}. \quad (5.56)$$

The same expression for the impedance is also obtained in cylindrical coordinates or planar Cartesian coordinates (not shown).

Note that if several ionic species are present, then the superposition principle applies (Fick equations are linear) and therefore the contribution of each ion will add up. The diffusion constants for different ions are of the same order of

magnitude (for Na^+ , K^+ , Cl^- , Ca^{2+}), so no particular ion would be expected to dominate.

5.7 Synthesis of the different models

In this section, we integrate the two phenomena, polarization and ionic diffusion, considered in previous sections, into a general macroscopic model. The objective of this synthesis is to analyze experimental results at macroscopic scales, and estimate the magnitude of the frequency dependence of the extracellular potential, as well as the respective influence of polarization and ionic diffusion. We will also mention other possible causes for frequency dependence in the discussion.

We consider below successively more complex models and how these models account for experimental data such as macroscopic measurements of conductivity.

5.7.1 Non-reactive media with ionic diffusion (model D)

Because current sources are ionic currents, there is flow of ions inside or outside the membrane, and another physical phenomenon underlying current flow is ionic diffusion. Let us consider a resistive medium such as a homogeneous extracellular conductive fluid in which the ionic diffusion coefficient is D . When the extracellular current is exclusively due to ionic diffusion, the current density depends on frequency as $\sqrt{\omega}$ (see Section 5.6.2). A resistive medium behaves as if it had a resistivity equal to $(1/\sigma^m)(1 + (k/\sqrt{\omega}))$, where b is complex. The parameter σ^m is the conductivity for very high frequencies, and reflects the fact that the effect of ionic diffusion becomes negligible compared to calorific dissipation (Ohm's law) for very high frequencies. When ionic diffusion is dominant compared to electric field effects, the real part of b is much larger than a .

The frequency dependence of conductivity will be given by:

$$\sigma_{\omega}^M = \frac{\sigma^m \sqrt{\omega}}{\sqrt{\omega} + k}. \quad (5.57)$$

Applying Equation (5.19) to this configuration gives the following expression for the electric potential as a function of distance:

$$V_{\omega}(\vec{r}) = \frac{1}{4\pi\sigma_z^M} \cdot \frac{I_{\omega}}{r} = \frac{\sqrt{\omega} + k}{\sqrt{\omega}} \cdot \frac{1}{4\pi\sigma^m} \cdot \frac{I_{\omega}}{r}. \quad (5.58)$$

This expression shows that, in a non-reactive medium, when the extracellular current is dominated by ionic diffusion ($k > \sqrt{\omega}$), then the impedance of the medium V_{ω}/I_{ω} will be frequency dependent and will scale as $1/\sqrt{\omega}$. This model will be

referred to as “model D” in the following. Note that if the electric field dominates over ionic diffusion, then we have the opposite situation, as described in Section 5.2.

5.7.2 Reactive media with electric fields (model P)

In reality, extracellular media contain different charge densities, for example because cells have a non-zero membrane potential by maintaining differences in ionic concentrations between the inside and outside of the cell. Such charge densities will necessarily be influenced by the electric field or by ionic diffusion. As above, we first consider the case with only electric field effects and will consider next the influence of diffusion and the two phenomena taken together.

Electric polarization is a prominent type of “reaction” of the extracellular medium to the electric field. In particular, the ionic charges accumulated over the surface of cells will migrate and polarize the cell under the action of the electric field. It was shown previously in a theoretical study that this “surface polarization” phenomenon can have important effects on the propagation of local field potentials (Bédard et al., 2006a). If a charged membrane is placed inside an electric field \vec{E}_0^S , there is production of a secondary electric field \vec{E}_ω^S given by (Bédard et al., 2006a):

$$\vec{E}_\omega^S = \frac{\vec{E}_0^S}{1 + i\omega\tau_{MW}}. \quad (5.59)$$

This expression is the frequency-domain representation of the effect of the inertia of charge movement associated with surface polarization, reflecting the fact that the polarization does not occur instantaneously but requires a certain time to set up. This frequency dependence of the secondary electric field was derived in Bédard et al. (2006a) for a situation where the current was exclusively produced by electric field. The parameter τ_{MW} is the characteristic time for charge movement (Maxwell–Wagner time) and equals $\epsilon^{memb}/\sigma^{memb}$, where ϵ^{memb} and σ^{memb} are respectively the absolute (tangential) permittivity and conductivity of the membrane surface, and are in general very different from the permittivity and the conductivity of the extracellular fluid.

Let us now determine for zero frequency the amplitude of the secondary field \vec{E}_0^S produced between two cells embedded in a given electric field. First, we assume that it is always possible to trace a continuous path which links two arbitrary points in the extracellular fluid (see Figure 5.12B). Consequently, the domain defined by extracellular fluid is said to be *linearly connex*. In this case, the electric potential arising from a current source is necessarily continuous in the extracellular fluid. Second, in a first approximation, we can consider that the cellular processes

surrounding sources are arranged randomly (as opposed to being regularly structured) and their distribution is therefore approximately isotropic. Consequently, the field produced by a given source in such a medium will also be approximately isotropic. Also consequent to this quasi-random arrangement, the equipotential surfaces around a spherical source will necessarily cut the cellular processes around the source (Figure 5.12B).

Because in complex Fourier analysis, the partials of the spectrum correspond to asymptotic states ($t \rightarrow \infty$), the zero-frequency component necessarily implies that the value of the charge is independent of time inside the cell (for a passive membrane). Thus, for zero frequency, there is a constant charge on cell surfaces such that the surface polarization is at steady state. This implies that the electric field inside the cells is zero (otherwise one would have a charge migration towards cell surface, which is in contradiction with the constant charge). Therefore, there cannot be a voltage difference between two equipotential surfaces (illustrated in Figure 5.12B). One can therefore conclude that *a passive inhomogeneous medium with randomly distributed passive cells is a perfect dielectric at zero frequency*. In this case, the conductivity must tend to 0 when frequency tends to 0. Thus, in the following, we assume that $\vec{E}_0^S = -\vec{E}_0^P$ where \vec{E}_0^P is the field produced by the source.

It follows that the expression for the current density in extracellular space as a function of the electric field is given by:

$$\vec{j}_\omega = \sigma_z^M \cdot \vec{E}_\omega^P = \sigma^m \cdot \vec{E}_\omega^{resul} = \sigma^m \cdot (\vec{E}^P + \vec{E}^S) = \sigma^m \cdot \frac{i\omega\tau_{MW}}{1 + i\omega\tau_{MW}} \cdot \vec{E}_\omega^P.$$

Thus, the conductivity can be written as:

$$\sigma_z^M = \sigma^m \cdot \frac{i\omega\tau_{MW}}{1 + i\omega\tau_{MW}}. \quad (5.60)$$

Applying Equation (5.19) gives:

$$V_\omega(\vec{r}) = \frac{1}{4\pi\sigma_z^M} \cdot \frac{I_\omega}{r} = \frac{i\omega\tau_{MW}}{1 + i\omega\tau_{MW}} \cdot \frac{1}{4\pi\sigma^m} \cdot \frac{I_\omega}{r}. \quad (5.61)$$

This model describes the effect of polarization in reaction to the source electric field, and will be referred to as “model P” in the following.

5.7.3 Reactive media with electric field and ionic diffusion (model DP)

The propagation of current in the medium is dominated by ionic diffusion currents or by currents produced by the electric field, according to the values of k and k_1 with respect to $\sqrt{\omega}$. The values of k and k_1 are respectively inversely proportional

to the square root of the global ionic diffusion coefficient in the extracellular fluid, and of the membrane surface (see Section 5.6.2).

We apply the reasoning based on the connex topology of the cortical medium (see above) to deduce the order of magnitude of the induced field for zero frequency \vec{E}_0^S

$$\vec{E}_\omega^S = -\frac{\vec{E}_0^P}{1 + i\sqrt{\omega}\tau}. \quad (5.62)$$

where

$$\tau = (\sqrt{\omega} + k_1)\tau_{MW} = \sqrt{\omega}\frac{\epsilon^{memb}}{\sigma^{memb}}.$$

Because the “tangential” conductivity on membrane surface is given by

$$\sigma_\omega^{memb} = \frac{\sigma^{Memb}\sqrt{\omega}}{\sqrt{\omega} + k_1}$$

when the current is dominated by either electric field or ionic diffusion (see Equation (5.57)).

It follows that the expression for the current density in extracellular space as a function of the electric field is given by

$$\vec{j}_\omega = \sigma_z^M \vec{E}_\omega^P = \sigma_\omega^M \cdot \left(1 + i\frac{\omega\epsilon_\omega^M}{\sigma_\omega^M}\right) \cdot \vec{E}_\omega^{resul} = \frac{\sigma^m\sqrt{\omega}}{\sqrt{\omega} + k} \cdot \left(1 + i\frac{\omega\epsilon_\omega^M}{\sigma_\omega^M}\right) \cdot (\vec{E}^P + \vec{E}^S).$$

We then obtain

$$\vec{j}_\omega \approx \frac{\sigma^m\sqrt{\omega}}{\sqrt{\omega} + k} \cdot \frac{i\sqrt{\omega}\tau}{1 + i\sqrt{\omega}\tau} \cdot \vec{E}_\omega^P$$

because $1 + i(\omega\epsilon_\omega^M/\sigma_\omega^M) \approx 1$ in cortical tissue for frequencies greater than 10 Hz and less than 1000 Hz (see Gabriel et al., 1996b).

Thus, we have the following expression for the complex conductivity of the extracellular medium:

$$\sigma_z^M \approx \frac{\sigma^m\sqrt{\omega}}{\sqrt{\omega} + k} \cdot \frac{i\sqrt{\omega}\tau}{1 + i\sqrt{\omega}\tau}. \quad (5.63)$$

where $\tau = (\sqrt{\omega} + k_1)\tau_{MW}$.

Thus, we have obtained a unique expression (Equation (5.63)) for the apparent conductivity in extracellular space outside of the source, and its frequency dependence due to differential Ohm’s law, electric polarization phenomena and ionic diffusion. These phenomena are responsible for an apparent frequency dependence of the electric parameters, which will be compared to the frequency dependence observed in macroscopic measurements of conductivity (Section 5.8).

Finally, Equations (5.19) and (5.63) imply that the macroscopic impedance of a homogeneous spherical shell of width $R_2 - R_1$ is given by:

$$Z_\omega \approx \frac{1}{4\pi} \int_{R_1}^{R_2} \frac{1}{r'^2} \frac{dr'}{\sigma_\omega^M + i\omega\epsilon_\omega^M} = \frac{R_2 - R_1}{4\pi R_1 R_2} \cdot \frac{1}{\sigma_\omega^M}. \quad (5.64)$$

In the following, this model will be referred as the “diffusion-polarization” model, or “DP” model, and we will use the above expressions (Equations (5.63) and (5.64)) to simulate experimental measurements.

5.8 Application of non-resistive LFP models to experimental data

One of the great advantages of the macroscopic LFP model is not only that it allows integration of different physical characteristics such as non-uniform media, electric polarization and ionic diffusion, but also it can directly integrate experimental measurements of conductivity. In this section, we consider two applications to illustrate the use of this model to interpret experimental data and suggest physical phenomena which are consistent with the experimental measurements.

5.8.1 Macroscopic measurements of brain conductivity

A first application of the formalism is to reproduce the macroscopic measurements of conductivity in brain tissue. The experiments of Gabriel et al., published in three companion papers (Gabriel et al., 1996a, 1996b, 1996c), provided a comprehensive set of measurements of conductivity in different biological media. In these experiments, the biological tissue was placed between two capacitor plates, and a sinusoidal current of frequency ω was applied. This setup was used to measure the capacitance and leak current using the relation $I_\omega = YV_\omega$, imposing the same current amplitude at all frequencies. Because the admittance value is proportional to $\sigma_\omega^M + i\omega\epsilon_\omega^M$, measuring the admittance provides direct information about σ_ω^M and ϵ_ω^M . In the case of brain tissue, these experiments revealed that the electric parameters were strongly dependent on frequency (Figure 5.13, curve G).

To stay consistent with the formalism developed above, we will assume that the capacitor has a spherical geometry. The exact geometry of the capacitor should in principle have no influence on the frequency dependence of the admittance, because the geometry will only affect the proportionality constant between σ_z and Y_ω . In the case of a spherical capacitor, by applying Equation (5.64), we obtain:

$$Y_\omega = \frac{1}{R} + i\omega C = 4\pi \frac{R_1 R_2}{R_2 - R_1} [\sigma_\omega^M + i\omega\epsilon_\omega^M] = 4\pi \frac{R_1 R_2}{R_2 - R_1} \sigma_z^M. \quad (5.65)$$

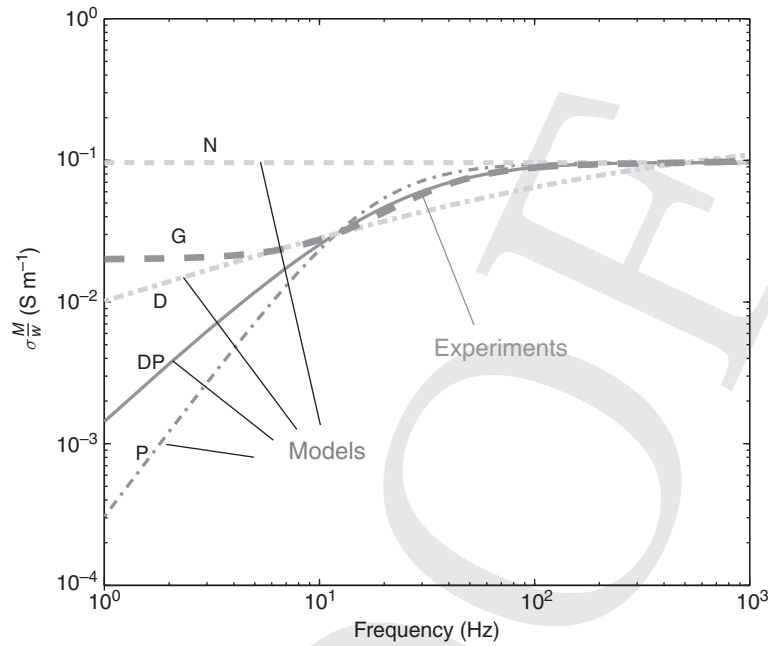


Figure 5.13 Models of macroscopic extracellular conductivity compared to experimental measurements in the cerebral cortex. The experimental data (labeled “G”) show the real part of the conductivity measured in cortical tissue by the experiments of Gabriel et al. (1996b). The curve labeled “N” represents the macroscopic conductivity calculated according to the effects of electric field in a non-reactive medium. The curve labeled “D” is the macroscopic conductivity due to ionic diffusion in a non-reactive medium. The curve labeled “P” shows the macroscopic conductivity calculated from a reactive medium with electric-field effects (polarization phenomena). The curve labeled “DP” shows the macroscopic conductivity in the full model, combining the effects of electric polarization and ionic diffusion. Each model was fit to the experimental data using a least-square procedure, and the best fit is shown. The DP model’s conductivity is given by $\frac{1}{\sigma_{\omega}^M} = K_0 + \frac{K_1}{f^{1/2}} + \frac{K_2}{f} + \frac{K_3}{f^{3/2}}$, with $K_0 = 10.84$, $K_1 = -19.29$, $K_2 = 180.35$ and $K_3 = 52.56$. The experimental data (G) is the parametric Cole–Cole model (Cole and Cole, 1941) which was fit to the experimental measurements of Gabriel et al. (1996b). This fit is in agreement with experimental measurements for frequencies larger than 10 Hz. No experimental measurements exist for frequencies lower than 10 Hz, and for those frequencies, the different curves show different predictions from the phenomenological model of Cole–Cole and the present models.

We also take into account the fact that the resistive part is always greater than the reactive part for low frequencies (less than 1000 Hz), which is expressed by

$$\omega \epsilon_{\omega}^M / \sigma_{\omega}^M \ll 1.$$

5 Modeling LFPs and interaction with extracellular medium

181

This relation can be verified for example from the Gabriel et al. (1996b) measurements, where it is valid for the whole frequency band investigated experimentally (between 10 and 10^{10} Hz).

The real part of $\sigma_{\omega}^M = \sigma_z$ then takes the form

$$\sigma_{\omega}^M \approx \frac{\sigma^M \sqrt{\omega}}{\sqrt{\omega} + k} \cdot \frac{\omega \tau^2}{\omega \tau^2 + 1} \quad (5.66)$$

where $\tau = (\sqrt{\omega} + k_1) \tau_{MW}$.

By substituting this value of τ , the inverse of the conductivity (the resistivity) is given by:

$$\frac{1}{\sigma_{\omega}^M} \approx \frac{1}{\sigma^M} \cdot \left(1 + \frac{k}{\sqrt{\omega}}\right) \cdot \left(1 + \frac{1}{\omega \tau_M^2 (\sqrt{\omega} + k_1)^2}\right). \quad (5.67)$$

Rearranging these terms, we can write:

$$\frac{1}{\sigma_{\omega}^M} \approx \frac{1}{\sigma^M} \cdot \left[1 + \frac{k}{\sqrt{\omega}} + \left(\frac{1}{\omega \tau_M^2} + \frac{k}{\omega^{3/2} \tau_M^2}\right) \left(\frac{1}{\omega + 2k_1 \sqrt{\omega} + k_1^2}\right)\right].$$

Finally, by assuming that the current produced by the electric field on membrane surfaces is negligible compared to the current produced by ionic diffusion, we have $k_1 \gg \sqrt{\omega}$ and by developing in series, the last term (in parentheses) of the last equation, we have:

$$\frac{1}{\sigma_{\omega}^M} \approx \bar{K}_0 + \frac{\bar{K}_1}{\omega^{1/2}} + \frac{\bar{K}_2}{\omega} + \frac{\bar{K}_3}{\omega^{3/2}} = K_0 + \frac{K_1}{f^{1/2}} + \frac{K_2}{f} + \frac{K_3}{f^{3/2}}. \quad (5.68)$$

Equation (5.68) corresponds to the conductivity σ^M , as measured under the experimental conditions of Gabriel et al. (the permittivity ϵ^M is obtained by applying Kramers–Kronig relations). Figure 5.13 shows that this expression for the conductivity can explain the measurements in the frequency range of 10 to 1000 Hz, which are relevant for LFPs. To obtain this agreement, we had to assume in Equation (5.63) a relatively low Maxwell–Wagner time of the order of 0.15 s ($f_c = 1/(2\pi\tau_M)$ between 1 Hz and 10 Hz), $k_1 > \sqrt{\omega} > k$ (for frequencies smaller than 100 Hz).

Thus, the model predicts that in the Gabriel et al. experiments, the transformation of electric current carried by electrons to ionic current in the biological medium necessarily implies an accumulation of ions at the plates of the capacitor. This ion accumulation will in general depend on frequency, because the conductivity and permittivity of the biological medium are frequency dependent. This will create a concentration gradient across the biological medium, which will cause an ionic diffusion current opposite to the electric current. This ionic current will allow a greater resulting current because surface polarization is opposite to the

electric field. Figure 5.13 shows that such conditions give frequency-dependent macroscopic parameters consistent with the measurements of Gabriel et al.

The choice of parameter needed to obtain this agreement can be justified qualitatively because the ionic diffusion constant on cellular surfaces is probably much smaller than in the extracellular fluid, such that $k_1 \gg k$. This implies the existence of a frequency band B_f for which $\sqrt{\omega}$ is negligible with respect to k_1 , but not with respect to k because these constants are inversely proportional to the square root of their respective diffusion coefficients. Thus, the approximation that we suggest here is that this band B_f finishes around 100 Hz in the Gabriel et al. experimental conditions. It is important to note that this parameter choice is entirely dependent on the ratio between the ionic diffusion current and the current produced by the electric field, and thus will depend on the particular experimental conditions.

It is interesting to note that the present model and the phenomenological Cole–Cole model (Cole and Cole, 1941) predict different behaviors of the conductivity for low frequencies (less than 10 Hz). In the present model, the conductivity tends to zero when the frequency tends to zero, while in the Cole–Cole extrapolation, it tends to a constant value (Gabriel et al., 1996a). The main difference between these models is that the Cole–Cole model is phenomenological and has never been deduced from physical principles for low frequencies, unlike the present model which is entirely deduced from well-defined physical phenomena.

5.8.2 Frequency dependence of the power spectral density of local field potentials

A second type of application of the formalism is to model the frequency dependence of LFPs. As outlined in the introduction (see Figure 5.1), the power spectral density (PSD) of LFPs or EEG signals displays $1/f$ frequency scaling (Bhattacharya and Petshe, 2001; Bédard et al., 2006a; Novikov et al., 1997; Pritchard, 1992). To examine whether this $1/f$ scaling can be accounted for by the present formalism, we consider a spherical current source embedded in a continuous macroscopic medium. We also assume that the PSD of the current source is a Lorentzian, which could derive for example from randomly occurring exponentially decaying postsynaptic currents (Bédard et al., 2006b) (see Figure 5.14).

To simulate this situation we used the “diffusion-polarization” (DP) model with ionic diffusion and electric field effects in a reactive medium. We have estimated above that surface polarization phenomena have a cut-off frequency of the order of 1 Hz, and will not play a role above that frequency. So, if we focus on the PSD of extracellular potentials in the frequency range larger than 1 Hz, we can consider only the effect of ionic diffusion (in agreement with the Gabriel et al. experiments, see above).

5 Modeling LFPs and interaction with extracellular medium

183

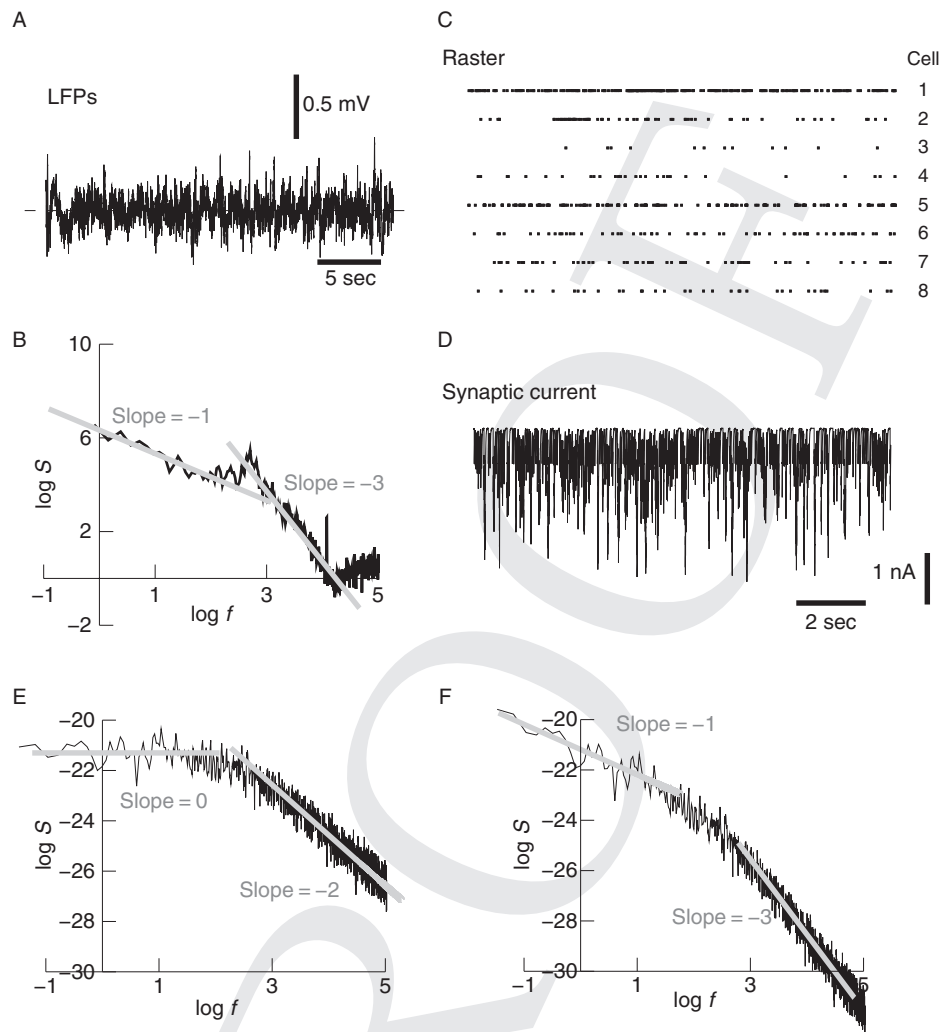


Figure 5.14 Simulation of $1/f$ frequency scaling of LFPs. A. LFP recording in the parietal cortex of an awake cat. B. Power spectral density (PSD) of the LFP on a log scale, showing two different scaling regions with a slope of -1 and -3 , respectively. C. Raster of eight simultaneously recorded neurons in the same experiment as in A. D. Synaptic current calculated by convolving the spike trains in C with exponentials (decay time constant of 10 ms). E. PSD calculated from the synaptic current, showing two scaling regions of slope 0 and -2 , respectively. F. PSD calculated using a model including ionic diffusion (see text for details). The scaling regions are of slope -1 and -3 , respectively, as in the experiments in B. Experimental data taken from Destexhe et al. (1999a); see also Bédard et al. (2006b) for details of the analysis in B–D.

Thus, we can approximate the conductivity as (see Equation (5.63)):

$$\sigma_{\omega}^M = a\sqrt{\omega} \quad (5.69)$$

where a is a constant.

It follows that the extracellular voltage around a spherical current source is given by (see Equation (5.19)):

$$V(r, \omega) = \frac{I_{\omega}}{4\pi a\sqrt{\omega} r} = \frac{V(r, 1)}{\sqrt{\omega}} = \frac{V(R, 1)R}{r\sqrt{\omega}} \quad (5.70)$$

where R is the radius of the source.

In other words, we can say that the extracellular potential is given by the current source I_{ω} convolved with a filter in $1/\sqrt{\omega}$, which is essentially due to ionic diffusion (Warburg impedance; see Hooge, 1962; Hooge and Bobbert, 1997; Diard et al., 1999). A white noise current source will thus result in a PSD scaling as $1/f$, and can explain the experimental observations, as shown in Figure 5.14. Experimentally recorded LFPs in cat parietal cortex display LFPs with frequency scaling as $1/f$ for low frequencies, and $1/f^3$ for high frequencies (Figure 5.14A, B). Following the same procedure as in Bédard et al. (2006b), we reconstructed the synaptic current source from experimentally recorded spike trains (Figure 5.14C, D). The PSD of the current source scales as a Lorentzian (Figure 5.14E) as expected from the exponential nature of synaptic currents. Calculating the LFP around the source and taking into account ionic diffusion, gives a PSD with two frequency bands, scaling as $1/f$ for low frequencies, and $1/f^3$ for high frequencies (Figure 5.14F). This is the frequency scaling observed experimentally for LFPs in awake cat cortex (Bédard et al., 2006b). We conclude that ionic diffusion is a plausible physical cause of the $1/f$ structure of LFPs for low frequencies.

5.9 Discussion

In the present chapter, we have proposed a framework to model local field potentials, which synthesizes previous measurements and models. This framework integrates microscopic measurements of electric parameters (conductivity σ and permittivity ϵ) of extracellular fluids, with macroscopic measurements of those parameters (σ_{ω}^M , ϵ_{ω}^M) in cortical tissue (Gabriel et al., 1996b; Logothetis et al., 2007). It also integrates previous models of LFPs, such as the *continuum model* (Bédard et al., 2004), which was based on a continuum hypothesis of variations of electric parameters in extracellular space, the *polarization model* (Bédard et al., 2006a) and models including the phenomenon of ionic diffusion (Bédard and Destexhe, 2009). The latter models explicitly considered different media (fluid and membranes), their polarization by current sources, and the mode of propagation

of current field in the medium. This “diffusion-polarization” model also accounts for observations of $1/f$ frequency scaling of LFP power spectra, which is due here to ionic diffusion, and is therefore predicted to be a consequence of the genesis of the LFP signal, rather than being solely due to neuronal activity (see bedard et al., 2006a). Finally, this work suggests that ephaptic interactions between neurons can occur not only through electric fields and that ionic diffusion should also be considered in such interactions.

An additional source of frequency dependence, not considered here, is the complex neuronal morphology (Pettersen and Einevoll, 2008). Even in a homogeneous and resistive medium, the neuronal morphology can influence the frequency dependence, as occurs for example for dipoles. Each monopole is responsible for a $1/r$ frequency dependence, which will be seen in the immediate vicinity of the monopole. For larger distances, at first approximation, the neuron acts as a linear combination of a dipole and a quadrupole, which gives a distance dependence as $a/r^2 + b/r^4$ (see Section 5.2).

Pettersen and Einevoll (2008) have pointed out that there is necessarily a frequency dependence of extracellular potential even in a homogeneous medium when the morphology is taken into account. In this case, the attenuation law produced by the soma is $1/r$, while that produced by currents distributed in dendrites will contribute as $a/r^2 + b/r^3$ (with respect to the “center” of the dendritic arbor). There is also an inherent frequency dependence of the signal propagation along dendrites (low-pass filter of the membrane RC circuit), such that the potential at a given position is approximately given by

$$\frac{A(f)}{r_{soma}} + B(f) \left[\frac{a}{r_{center}^2} + \frac{b}{r_{center}^3} \right]$$

where $A(f)$ and $B(f)$ are two different functions. Thus, the frequency dependence will be different according to position; near the soma, the $1/r$ term will be dominant, while closer to the “center” of dendrites, the term $a/r_{center}^2 + b/r_{center}^3$ will be the dominant one. Note that, as shown in Chapter 4, if the neuron is described by an ideal dipole, the two functions $A(f)$ and $B(f)$ will be equal, such that there will be no frequency dependence due to position.

It is important to note that such effects will only be prominent at fast frequencies. At frequencies less than 10Hz, the difference between functions A and B will become negligible because the effects due to propagation delay on the dendritic arbor will be very small. Thus, the Pettersen and Einevoll (2008) model cannot explain the $1/f$ spectral structure of LFPs and EEGs, which are most prominent for slow frequencies (see Figure 5.1).

We also investigated ways to explain the measurements of Logothetis et al. (2007), who reported that the extracellular medium was resistive and therefore

did not display frequency dependence, in contradiction with the measurements of Gabriel et al. (1996b). We summarize and discuss our conclusions below.

In the experiments of Gabriel et al. (1996b), permittivity and conductivity were measured in the medium in between two metal plates. This forms a capacitor, for which a (macroscopic) complex impedance is measured. This measure actually consists of two independent measurements, the real and imaginary parts of the impedance. These values are used to deduce the macroscopic permittivity and macroscopic conductivity of the medium. However, at the interface between the medium and the metal plates, the flow of electrons in the metal corresponds to a flow of charges in the tissue, and a variety of phenomena can occur, which can interfere with the measurement. The accumulation of charges that occurs at the interface between the electrode and the extracellular fluid implies a polarization impedance, which depends on the interaction between ions and the metal plate. Because this accumulation of charge implies a variation of concentration, the flow of ions may involve an important component of ionic diffusion.

In the experiments of Logothetis et al., a system of four electrodes was used, the two extreme electrodes inject current in the medium, while the two electrodes in the middle are used exclusively to measure the voltage. This system is supposed to be more accurate than that of Gabriel et al., because the electrodes that measure voltage are not subject to charge accumulation. However, the drawback of this method is non-linear effects. The magnitude of the injected current is such that the voltage at the extreme electrodes saturates. This voltage saturation also implies saturation of concentration (capacitive effect between electrodes), which limits ionic diffusion currents. Thus, the ratio between ionic diffusion currents and the currents due to the electric field is greatly diminished relative to the experiments of Gabriel et al.

We think that natural current sources are closer to the situation of Gabriel et al. for several reasons. First, the magnitude of the currents produced by biological sources is far too low for saturation effects. Second, the flow of charges across ion channels will produce perturbations of ionic concentration, which will be re-equilibrated by diffusion. The effects may not be as strong as the perturbations of concentrations induced by Gabriel et al.'s type of experiments, but ionic diffusion should play a role in both cases. This is precisely one of the aspects that should be evaluated in further experiments.

The experiments of Logothetis et al. (2007) were done using a four-electrode setup which neutralizes the influence of electrode impedance on voltage measurements (McAdams and Jossinet, 1992; Geddes, 1997). This system was used to perform high-precision impedance measurements, also avoiding ionic diffusion effects (Logothetis et al., 2007). Indeed, these experimental conditions, and the apparent resistive medium, could be reproduced by the present model if ionic diffusion was neglected. The present model therefore formulates the strong prediction

that ionic diffusion is important, and that any measurement technique should allow ionic diffusion to reveal the correct frequency-dependent properties of impedance and electric parameters in biological tissue.

The main prediction of the present model is that ionic diffusion is an essential physical cause of the frequency dependence of LFPs. We have shown that the presence of ionic diffusion allows the model to account quantitatively for the macroscopic measurements of the frequency dependence of electric parameters in cortical tissue (Gabriel et al., 1996b). Ionic diffusion is responsible for a frequency dependence of the impedance as $1/\sqrt{\omega}$ for low frequencies (less than 1000 Hz), which accounts directly for the observed $1/f$ frequency scaling of LFP and EEG power spectra during wakefulness (Pritchard, 1992; Novikov et al., 1997; Bhattacharya and Petsche, 2001; Bédard et al., 2006a) (see Figure 5.14). Note that the EEG is more complex because it depends on the propagation of the signal across fluids, dura mater, skull, muscles and skin. However, this filtering is of low-pass type, and may not affect the low-frequency band, so there is a possibility that the $1/f$ scaling of EEG and LFPs have a common origin. The present model is consistent with the view that this apparent “ $1/f$ noise” in brain signals is not generated by self-organized features of brain activity, but is rather a consequence of the genesis of the signal and its propagation through extracellular space (Bédard et al., 2006a). This is also in agreement with a recent study showing that the transfer function between simultaneously recorded intracellular and extracellular potentials is consistent with $1/f$ frequency filtering by extracellular media (Bédard et al., 2010).

It is important to note that the fact that ionic diffusion may be responsible for $1/f$ frequency scaling of LFPs is not inconsistent with other factors which may also influence frequency scaling. For example, the statistics of network activity – and more generally network state – can affect frequency scaling. This is apparent when comparing awake and slow-wave sleep LFP recordings in the same experiment, showing that the $1/f$ scaling is only seen in wakefulness but $1/f^2$ scaling is seen during sleep (Bédard et al., 2006a) (see Figure 5.14). In agreement with this, recent results indicate that the correlation structure of synaptic activity may influence frequency scaling at the level of the membrane potential, and that correlated network states scale with larger (more negative) exponents (Marre et al., 2007).

The critical question that remains to be solved is whether, under physiological conditions, ionic diffusion plays a role as important as that suggested here. We proposed a simple method to test this hypothesis (Bédard and Destexhe, 2009). The frequency dependence could be evaluated by using an extracellular electrode injecting current in conditions as close as possible to physiological conditions (a micropipette would be appropriate). By measuring the integration of the extracellular voltage following periodic current injection, one could estimate the “relaxation

time” of the medium with respect to charge accumulation. If this relaxation time occurs at time scales relevant to neuronal currents (milliseconds) rather than the fast relaxation predicted by a purely resistive medium (picoseconds), then ionic diffusion will necessarily occur under physiological conditions, which would provide evidence in favor of the present mechanism.

Finally, our study predicts that the impedance tends to zero when the frequency tends to zero. Thus, for slow frequencies, the extracellular electric field can become very large, and perhaps creates significant ephaptic interactions. It is tempting to relate this to the observation that slow frequencies are more synchronized in general compared to fast frequencies (Bullock, 1997; Destexhe et al, 1999a). Hypersynchronized phenomena, such as epileptic or suppression burst EEG patterns, are usually of slow frequency. These observations also support the notion that frequency dependence is a fundamental property of the propagation of extracellular potentials.

Acknowledgments

This research was supported by the CNRS, the ANR (HR-Cortex) and the European Community (projects FACETS and BrainScales).

References

- Bhattacharya, J. and Petsche, H. (2001). Universality in the brain while listening to music. *Proc. Biol. Sci.*, **268**, 2423–2433.
- Bédard, C. and Destexhe, A. (2009). Macroscopic models of local field potentials and the apparent $1/f$ noise in brain activity. *Biophys. J.*, **96**, 2589–2603.
- Bédard, C., Kröger, H. and Destexhe, A. (2004). Modeling extracellular field potentials and the frequency-filtering properties of extracellular space. *Biophys. J.*, **86**, 1829–1842.
- Bédard, C., Kröger, H. and Destexhe, A. (2006a). Model of low-pass filtering of local field potentials in brain tissue. *Phys. Rev. E*, **73**, 051911.
- Bédard, C., Kröger, H. and Destexhe, A. (2006b). Does the $1/f$ frequency scaling of brain signals reflect self-organized critical states? *Phys. Rev. Lett.*, **97**, 118102.
- Bédard, C. and Destexhe, A. (2008). A modified cable formalism for modeling neuronal membranes at high frequencies. *Biophys. J.*, **94**, 1133–1143.
- Bédard, C., Rodrigues, S., Roy, N., Contreras, D. and Destexhe, A. (2010). Evidence for frequency-dependent extracellular impedance from the transfer function between extracellular and intracellular potentials. *J. Comput. Neurosci.*, **29**, 389–403.
- Beggs, J. and Plenz, D. (2003). Neuronal avalanches in neocortical circuits. *J. Neurosci.*, **23**, 11167–11177.
- Braitenberg, V. and Shüz, A. (1998). *Cortex: Statistics and Geometry of Neuronal Connectivity* (2nd edition). Berlin: Springer-Verlag.
- Bremer, F. (1938). L'activité électrique de l'écorce cérébrale. *Actual. Sci. Ind.* **658**, 3–46.
- Bremer, F. (1949). Considérations sur l'origine et la nature des “ondes” cérébrales. *Electroencephalogr. Clin. Neurophysiol.*, **1**, 177–193.

- Buckingham, M. J. J. (1985). *Noise in Electronic Devices and Systems*. New York: John Wiley & Sons.
- Bullock, T. H. (1997). Signals and signs in the nervous system: the dynamic anatomy of electrical activity is probably information-rich. *Proc. Natl. Acad. Sci. USA*, **94**, 1–6.
- Cajal, R. (1909). *Histologie du Système Nerveux de l'Homme et des Vertébrés*. Paris: Maloine.
- Cole, K. S. and Cole, R. H. (1941). Dispersion and absorption in dielectrics I. Alternating current characteristics. *J. Chem. Phys.*, **9**, 341–351.
- Creutzfeldt, O., Watanabe, S. and Lux, H. D. (1966a). Relation between EEG phenomena and potentials of single cortical cells. I. Evoked responses after thalamic and epicortical stimulation. *Electroencephalogr. Clin. Neurophysiol.*, **20**, 1–18.
- Creutzfeldt, O., Watanabe, S. and Lux, H. D. (1966b). Relation between EEG phenomena and potentials of single cortical cells. II. Spontaneous and convulsoid activity. *Electroencephalogr. Clin. Neurophysiol.*, **20**, 19–37.
- Debye, P. and Hückel, E. (1923). The theory of electrolytes. I. Lowering of freezing point and related phenomena. *Phys. Z.*, **24**, 185–206.
- Destexhe, A. (1998). Spike-and-wave oscillations based on the properties of GABA_B receptors. *J. Neurosci.*, **18**, 9099–9111.
- Destexhe, A. and Paré, D. (1999). Impact of network activity on the integrative properties of neocortical pyramidal neurons in vivo. *J. Neurophysiol.*, **81**, 1531–1547.
- Destexhe, A., Contreras, D. and Steriade, M. (1999a). Spatiotemporal analysis of local field potentials and unit discharges in cat cerebral cortex during natural wake and sleep states. *J. Neurosci.*, **19**, 4595–4608.
- Destexhe, A., McCormick, D. A. and Sejnowski, T. J. (1999b). Thalamic and thalamocortical mechanisms underlying 3 Hz spike-and-wave discharges. *Prog. Brain Res.* **121**, 289–307.
- Diard, J.-P., Le Gorrec, B. and Montella, C. (1999). Linear diffusion impedance. General expression and applications. *J. Electroanal. Chem.*, **471**, 126–131.
- Eccles, J. C. (1951). Interpretation of action potentials evoked in the cerebral cortex. *J. Neurophysiol.*, **3**, 449–464.
- Foster, K. R. and Schwan, H. P. (1989). Dielectric properties of tissues and biological materials: a critical review. *Crit. Rev. Biomed. Eng.*, **17**, 25–104.
- Gabriel, S., Lau, R. W. and Gabriel, C. (1996a). The dielectric properties of biological tissues: I. Literature survey. *Phys. Med. Biol.*, **41**, 2231–2249.
- Gabriel, S., Lau, R. W. and Gabriel, C. (1996b). The dielectric properties of biological tissues: II. Measurements in the frequency range 10 Hz to 20 GHz. *Phys. Med. Biol.*, **41**, 2251–2269.
- Gabriel, S., Lau, R. W. and Gabriel, C. (1996c). The dielectric properties of biological tissues: III. Parametric models for the dielectric spectrum tissues. *Phys. Med. Biol.* **41**, 2271–2293.
- Geddes, L. A. (1997). Historical evolution of circuit models for the electrode–electrolyte interface. *Ann. Biomed. Eng.*, **25**, 1–14.
- Hille, B. (2001). *Ion Channels and the Excitable Membranes* (3rd edition). Sunderland, MA: Sinauer.
- Hines, M. L. and Carnevale, N. T. (2000). The NEURON simulation environment. *Neural Comput.*, **9**, 1179–1209.
- Hooge, F. N. (1962). $1/f$ noise is no surface effect. *Phys. Lett.*, **29A**, 139–140.
- Hooge, F. N. and Bobbert, P. A. (1997). On the correlation function of $1/f$ noise. *Physica B*, **239**, 223–230.

- Jensen, H. J. (1998). *Self-Organized Criticality: Emergent Complex Behavior in Physical and Biological Systems*. Cambridge: Cambridge University Press. UK.
- Johnston, D. and Wu, S. M.-S. (1999). *Foundation of Cellular Neurophysiology*. Cambridge, MA: MIT Press.
- Katzner, S., Nauhaus, I., Benucci, A., Bonin, V., Ringach, D. L. and Carandini, M. (2009). Local origin of field potentials in visual cortex. *Neuron.*, **61**, 35–41.
- Klee, M. and Rall, W. (1977). Computed potentials of cortically arranged populations of neurons. *J. Neurophysiol.*, **40**, 647–666.
- Klee, M. R., Offenloch, K. and Tigges, J. (1965). Cross-correlation analysis of electroencephalographic potentials and slow membrane transients. *Science* **147**, 519–521.
- Koch, C. (1999). *Biophysics of Computation*. Oxford: Oxford University Press.
- Koch, C. and Segev, I. (editors) (1998). *Methods in Neuronal Modeling* (2nd edition). Cambridge MA: MIT Press.
- Kronig, R. D. L. (1926). On the theory of dispersion of X-rays. *J. Opt. Soc. Am.*, **12**, 547.
- Logothetis, N. K., Kayser, C. and Oeltermann, A. (2007). In vivo measurement of cortical impedance spectrum in monkeys: Implications for signal propagation. *Neuron*, **55**, 809–823.
- Landau, L. D. and Lifshitz, E. M. (1984). *Electrodynamics of Continuous Media*. Oxford: Pergamon Press.
- Marre, O., El Boustani, S., Baudot, P., Levy, M., Monier, C., Huguet, N., Pananceau, M., Fournier, J., Destexhe, A. and Frégnac, Y. (2007). Stimulus-dependency of spectral scaling laws in V1 synaptic activity as a read-out of the effective network topology. *Soc. Neurosci. Abstr.*, **33**, 790.6.
- Maxwell, J. C. (1873). *A Treatise on Electricity and Magnetism*, Chapter 10, pp. 374–375. Oxford: Clarendon Press.
- McAdams, E. T. and Jossinet, J. (1992). A physical interpretation of Schwan's limit current of linearity. *Ann. Biomed. Eng.*, **20**, 307–319.
- Nicholson, C. (2005). Factors governing diffusing molecular signals in brain extracellular space. *J. Neural Transm.*, **112**, 29–44.
- Nicholson, C. and Sykova, E. (1998). Extracellular space structure revealed by diffusion analysis. *Trends Neurosci.*, **21**, 207–215.
- Niedermeyer, E. and Lopes da Silva, F. (editors) (1998). *Electroencephalography* (4th edition). Baltimore, MD: Williams and Wilkins.
- Novikov, E., Novikov, A., Shannahoff-Khalsa, D., Schwartz, B. and Wright, J. (1997). Scale-similar activity in the brain. *Phys. Rev. E*, **56**, R2387–R2389.
- Nunez, P. L. (1981). *Electric Fields of the Brain. The Neurophysics of EEG*. Oxford: Oxford University Press.
- Nunez, P. L. and Srinivasan, R. (2005). *Electric Fields of the Brain* (2nd edition). Oxford: Oxford University Press.
- Nyquist, H. (1928). Thermal agitation of electric charge in conductors. *Phys. Rev.*, **32**, 110–113.
- Peters, A., Palay, S. L. and Webster, H. F. (1991). *The Fine Structure of the Nervous System*. Oxford: Oxford University Press.
- Pethig, R. (1979). *Dielectric and Electronic Properties of Biological Materials*. New York: John Wiley & Sons.
- Pettersen, K. H. and Einevoll, G. T. (2008). Amplitude variability and extracellular low-pass filtering of neuronal spikes. *Biophys. J.*, **94**, 784–802.
- Pritchard, W. S. (1992). The brain in fractal time: $1/f$ -like power spectrum scaling of the human electroencephalogram. *Int. J. Neurosci.*, **66**, 119–129.

5 Modeling LFPs and interaction with extracellular medium

191

- Protopapas, A. D., Vanier, M. and Bower, J. (1998). Simulating large-scale networks of neurons. In: C. Koch and I. Segev (editions), *Methods in Neuronal Modeling* (2nd edition), pp. 461–498. Cambridge, MA: MIT Press.
- Purcell, E. M. (1984). *Electricity and Magnetism*. New York: McGraw Hill.
- Raju, G. G. (2003). *Dielectrics in Electric Fields*. New York: CRC Press.
- Rall, W. and Shepherd, G. M. (1968). Theoretical reconstruction of field potentials and dendrodendritic synaptic interactions in olfactory bulb. *J. Neurophysiol.*, **31**, 884–915.
- Ranck, J. B. (1963). Specific impedance of rabbit cerebral cortex. *Exp. Neurol.*, **7**, 144–152.
- Rusakov, D. A. and Kullmann, D. M. (1998). Geometric and viscous components of the tortuosity of the extracellular space in the brain. *Proc. Natl. Acad. Sci. USA*, **95**, 8975–8980.
- Steriade, M. (2003). *Neuronal Substrates of Sleep and Epilepsy*. Cambridge: Cambridge University Press.
- Taylor, S. R. and Gileadi, E. (1995). The physical interpretation of the Warburg impedance. *Corrosion*, **51**, 664–671.
- Vasilyev, A. M. (1983). *An Introduction to Statistical Physics*. Moscow: MIR Editions.